Increased apoptotic priming of glioblastoma enables therapeutic targeting by BH3-mimetics

Anna L Koessinger[1,2], Dominik Koessinger[1,2], Kevin Kinch[3], Laura Martínez-Escardó[2,4], Nikki R Paul[1], Yassmin Elmasry[2], Gaurav Malviya[1], Catherine Cloix[1,2], Kirsteen J Campbell[1,2], Florian J Bock[1,2], Jim O'Prey[1], Katrina Stevenson[2], Colin Nixon[1], Mark R Jackson[2], Gabriel Ichim[5], William Stewart[3], Karen Blyth[1,2], Kevin M Ryan[1,2], Anthony J Chalmers[2], Jim C Norman[1,2] and Stephen WG Tait[1,2] *

[1] CRUK Beatson Institute, Bearsden, Glasgow, G61 1BD, UK.

[2] Institute of Cancer Sciences, College of Medical, Veterinary and Life Sciences, University of Glasgow, Bearsden, Glasgow, G61 1QH, UK.

[3] Department of Neuropathology, Queen Elizabeth University Hospital and Institute of Neuroscience and Psychology, University of Glasgow, UK.

[4] Department of Biochemistry and Molecular Biology and Institute of Neurosciences, Faculty of Medicine, Universitat Autònoma de Barcelona, Barcelona, Spain.

[5] Cancer Research Centre of Lyon (CRCL) INSERM 1052, CNRS 5286, Lyon, France.

*To whom correspondence should be addressed: Stephen Tait

CRUK Beatson Institute, University of Glasgow, Glasgow, G61 1BD, UK

Email: stephen.tait@glasgow.ac.uk

Running title: Overcoming apoptotic resistance in GBM

Keywords: apoptosis/BH3-mimetics/glioblastoma/resistance/stem cells

Abstract

IDH wild-type glioblastoma (GBM) is the most prevalent malignant primary brain tumour in adults. GBM typically has a poor prognosis, mainly due to a lack of effective treatment options leading to tumour persistence or recurrence. Tackling this, we investigated the therapeutic potential of targeting anti-apoptotic BCL-2 proteins in GBM. Levels of anti-apoptotic BCL-xL and MCL-1 were consistently increased in GBM compared with non-malignant cells and tissue. Moreover, we found that relative to their differentiated counterparts, patient-derived GBM stem-like cells also displayed higher expression of anti-apoptotic BCL-2 family members. Surprisingly, high anti-apoptotic BCL-xL and MCL-1 expression correlated with heightened susceptibility of GBM to BCL-2 family protein-targeting BH3-mimetics. This is indicative of increased apoptotic priming. Indeed, GBM displayed an obligate requirement for MCL-1 expression in both tumour development and maintenance. Investigating this apoptotic sensitivity, we found that sequential inhibition of BCL-xL and MCL-1 led to robust anti-tumour responses *in vivo*, in the absence of overt toxicity. These data demonstrate that BCL-xL and MCL-1 pro-survival function is a fundamental prerequisite for GBM survival that can be therapeutically exploited by BH3-mimetics.

Introduction

In adults, *IDH* wild-type glioblastoma *(IDHwt* GBM) is the most prevalent and malignant primary brain tumour (1, 2). Despite current multimodal treatment, comprising surgical resection with adjuvant radiotherapy and alkylating chemotherapy, the median survival in newly diagnosed patients remains poor at less than 12 months (3, 4). Resistance to conventional radio- and chemotherapy primarily emerges from persistent cancer stem cells, a tumourigenic subpopulation of GBM cells, consisting of heterogenous subclones and capable of self-renewal (5, 6). Therefore, targeting cells with stem-like capabilities is essential to develop effective treatment options and improve patient survival.

Treatment resistance can often be attributed to cells circumventing therapy-induced cell death. Apoptosis is an evolutionarily conserved type of cell death with broad ranging importance in biology (7). The intrinsic (mitochondrial) pathway of apoptosis is controlled by pro- and anti-apoptotic members of the B cell lymphoma 2 (BCL-2) family that regulate mitochondrial outer membrane integrity (8). During apoptosis, pro-apoptotic BCL-2 proteins cause mitochondrial outer membrane permeabilisation or MOMP. This leads to the release of mitochondrial intermembrane space proteins, including cytochrome *c*, that activate caspase proteases leading to apoptotic cell death (8).

Increased anti-apoptotic BCL-2 protein expression has been described in a wide range of solid cancers and is often linked with insensitivity to conventional chemotherapy (9-11). Recently, a new class of chemotherapeutics called BH3-mimetics have been developed that target pro-survival BCL-2 function, sensitising to cell death. BH3-mimetics have proven to be highly effective in haematologic malignancies. For instance, venetoclax (ABT-199), a BCL-2 targeted BH3-mimetic (12), is in clinical use for chronic lymphocytic leukaemia (CLL) (13) and acute myelogenous leukaemia (AML) (14, 15). CLL cells typically express high levels of anti-apoptotic BCL-2 protein. Nevertheless, the high intrinsic apoptotic sensitivity - also called apoptotic priming - of CLL renders it sensitive to venetoclax. For solid cancers,

venetoclax is currently being tested in combination with conventional chemotherapeutic agents. The combination of venetoclax and tamoxifen has progressed to early phase clinical trials in patients with estrogen receptor positive (ER+), high BCL-2 expressing breast cancer (16). Other BH3-mimetics developed to target BCL-xL and MCL-1 have shown promising pre-clinical results in combination with inhibitors of MEK1/2 for solid cancers harbouring oncogenic mutations in the MAPK pathway (17-19). Approximately 10% of GBM carry a mutation of isocitrate dehydrogenase 1 (*IDH1*) (1), which has been linked with increased sensitivity to treatment with BH3-mimetics targeting BCL-xL (20). Furthermore, previous studies have proposed BCL-xL as a treatment target in combination with ionising radiation (21) and other chemotherapeutics (22) in GBM.

Because tumours retain characteristics of their tissue origins, brain derived glial cancers exhibit defined cellular hierarchies found in brain development and homeostasis (23-25). During central nervous system development, anti-apoptotic BCL-2 family proteins play a pivotal role in promoting cell survival (26, 27) while with adulthood the brain becomes refractive to apoptosis (28). Given this important role in cell survival, we hypothesised that GBM, while phenocopying the developing brain, might display similar anti-apoptotic survival dependencies. Indeed, we found increased levels of the major pro-survival proteins in GBM, specifically within the stem-cell enriched population. Surprisingly, high BCL-xL and MCL-1 expression correlates with increased apoptotic sensitivity, demonstrating that GBM stem-like cells are primed for apoptosis. Exploiting this, we found that sequential dosing of BCL-xL and MCL-1 targeting BH3-mimetics enables effective treatment responses both, *in vitro* and *in vivo*. This could offer a therapeutically tractable approach for patients with *IDHwt* GBM.

Results

High anti-apoptotic BCL-2 family protein expression correlates with increased BH3-mimetic sensitivity in GBM

Cancer stem cells are proposed to give rise to GBM and contribute to therapeutic resistance (23). We therefore sought to assess the apoptotic sensitivity of GBM stem-like cells (GSC) by treating them with BH3-mimetics with selectivity for BCL-2, BCL-xL and MCL-1. For this purpose, we used a panel of patient-derived *IDHwt* GSC, cultured under conditions to maintain their tumour specific phenotype and stem cell properties (29, 30). Cell viability was measured using IncuCyte live-cell imaging and SYTOX Green exclusion. Importantly, three cell lines (G1, G7 and R24 GSC) were sensitive to A-1331852, a selective BCL-xL antagonist (31) whereas two cell lines (R9 and R15 GSC) displayed sensitivity to S63845, a potent and selective MCL-1 inhibitor (32) (**Figure 1A,B**). Moreover, the commonly used GBM cell line U87MG displayed increased sensitivity to BCL-xL inhibition when cultured under stem cell-enriching conditions. One cell line (E2 GSC) was resistant to all single agent treatments. Treatment with venetoclax (ABT-199), a BCL-2 specific inhibitor, induced no more than 26% cell death in any GSC and therefore was comparably inefficient. Collectively, these data show that the majority of tested GSC display survival dependence on anti-apoptotic BCL-2 family function.

We next used immunoblotting to determine if the individual apoptotic sensitivity of the patient-derived GSC corresponded to anti-apoptotic BCL-2 protein expression. In comparison to human differentiated astrocytes, all GSC exhibited higher expression of BCL-xL and MCL-1 and partially higher expression of BCL-2 (**Figure 1C**). Consistent with their origins, GSC expressed higher levels of neural stem cell marker SOX2 (33), while cell lineage specific GFAP was more abundant in astrocytes (34). Subsequently, we investigated whether anti-apoptotic BCL-2 protein expression also differed in GBM tumours and adjacent brain tissue. Using immunohistochemistry (IHC) we compared BCL-xL and MCL-1 expression in matched specimens of three patients diagnosed with GBM. In all cases, MCL-1 and BCL-xL were increased in the tumour cores compared to the predominantly non-

tumorous margins (**Figure 1D,E**). Extending this analysis, we determined MCL-1 and BCL-xL mRNA expression in different glioma subtypes and normal brain tissue using the publicly available REMBRANDT database. In line with our IHC analysis, *BCL-xL* and *MCL-1* mRNA levels were more expressed in GBM compared with lower grade gliomas and normal brain tissue (**Supplementary Figure 1A,B**). These data demonstrate specific sensitivities of patient-derived GSC to individual BH3-mimetics and increased expression of anti-apoptotic BCL-2 proteins in both primary GBM tumour tissues and GSCs.

Anti-apoptotic MCL-1 is required for the growth and survival of GBM

While it has previously been shown that GBM tumoursphere formation is promoted by high BCL-xL expression (35), little is known about the role of MCL-1 on GBM growth and maintenance. To explore the importance of MCL-1 in GBM formation and growth *in vivo*, we selected a tumourigenic cell line (G7 GSC) and deleted *MCL-1* using CRISPR/Cas9 genome editing. Western blot analysis confirmed efficient *MCL-1* deletion, while the expression of BCL-xL, SOX2 and GFAP was increased in the MCL-1^{CRISPR} cells (**Supplementary Figure 2A**). MCL-1^{CRISPR} GSC were found to proliferate at the same rate and retained a similar capability to form neurospheres as their vector^{CRISPR} counterparts (**Figure 2A, Supplementary Figure 2B**). We next investigated whether MCL-1 was required for tumourigenesis *in vivo*. iRFP-labelled vector^{CRISPR} and MCL-1^{CRISPR} G7 GSC were orthotopically injected in CD-1 nude mice and tumour growth was monitored with cranial magnetic resonance imaging (MRI) and iRFP signal detection (36). We observed a substantial impairment of tumour growth in MCL-1 deleted tumours (**Figure 2B,C; Supplementary Figure 2C**) that was reflected in the significantly prolonged survival of these mice (**Figure 2D**). Importantly, IHC analysis of the end-stage tumours revealed an outgrowth of MCL-1 proficient tumour cells in the MCL-1^{CRISPR} xenografts (**Supplementary Figure 2D**). In contrast to the *in vitro* analysis, these data reveal a key role for MCL-1 in initiation and growth of GBM *in vivo* and identify MCL-1 as a promising therapeutic target. Our results also support an important pro-survival role for anti-apoptotic MCL-1 in GBM.

GSC display increased apoptotic priming and can be effectively killed by dual BCL-xL, MCL-1 inhibition

Currently, no treatment regimen is able to achieve long-time remission of GBM, with tumours inevitably developing resistance to treatment and recurring, eventually leading to patient death (37). Anti-apoptotic BCL-2 family members have overlapping binding affinities for several pro-apoptotic BH3-only proteins (8). We asked whether GBM might circumvent single inhibitor treatment by compensatory upregulation of untargeted anti-apoptotic proteins. Indeed, upon treatment with BCL-xL inhibitor A-1331852 or navitoclax (ABT-737), an inhibitor of BCL-xL, BCL-2 and BCL-w, we found that levels of MCL-1 protein were increased in surviving GSC (**Figure 3A, Supplementary Figure 3A**). We reasoned that GBM might counteract drug-induced neutralisation of BCL-xL function via increased MCL-1 expression. To address this, we treated MCL-1^{CRISPR} G7 and R24 GSC with the BCL-xL inhibitors A-1331852 or ABT-263. Cell viability was measured by live-cell IncuCyte imaging with Sytox Green exclusion or in a clonogenic survival assay. In all cases, MCL-1 deletion significantly increased cellular sensitivity to the BCL-xL specific antagonist and navitoclax (**Figure 3B, Supplementary Figure 3B**). Similarly, dual inhibition of BCL-xL and MCL-1 with A-1331852 and S63845 displayed a substantial combinatorial effect resulting in up to 100% cell death across a range of GSC, determined in both short term cell viability assays and long-term clonogenic survival assays (**Figure 3C,D; Supplementary Figure 3C,D**). This effect was observed even at 10-fold decreased doses compared to effective single treatment. Verifying on-target engagement of mitochondrial apoptosis, combined MCL-1 and BCL-xL inhibition led to Caspase 3 and PARP-1 cleavage as well as cell death in a BAK, BAX and caspase-dependent manner (**Figure 3E, Supplementary Figures 3E-F**).

Sensitivity of GBM cells to chemotherapy and ionising radiation inversely correlates with tumour cell stemness (6, 38, 39). We therefore hypothesised that the differentiated counterparts (DIFF) of the patient-derived GBM stem-like cells may be more sensitive towards BH3-mimetic treatment. To ensure comparable culture conditions for GSC and

DIFF, we conducted these experiments using 1% FCS containing Ad-DMEM medium during the experimental procedure. Cells were treated with A-1331852 and S63845 to inhibit BCL-xL and MCL-1 respectively and cell viability measured by live-cell IncuCyte imaging and Sytox Green exclusion. Following treatment with single BH3-mimetic, we found that cell viability was largely comparable for DIFF and GSC (**Supplementary Figure 3G**). Surprisingly, following dual MCL-1 and BCL-xL inhibition, E2 and R15 GSC were more sensitive than DIFF cells; while >50% cell death was observed within about 5 hours in GSC, it was not observed in DIFF cells until 16 hours (**Figure 3F**). Moreover, 100% cell death was not achieved in either of the DIFF cell lines. Together, these data suggest that GSCs are more primed for apoptotic cell death than DIFF cells. To investigate this further, we compared expression of pro- and anti-apoptotic BCL-2 proteins in the paired cell lines. Although more sensitive to apoptosis, GSCs displayed higher levels of anti-apoptotic BCL-2 proteins, BCL2, BCL-xL and MCL-1 than their differentiated counterparts (**Supplementary Figure 3H**). In summary, these data indicate that GSC can display increased apoptotic priming and reveal potent cytotoxic effects of dual-targeting BCL-xL and MCL-1.

TrkB signalling regulates sensitivity of GSC to anti-apoptotic treatment

We next sought to explore the differential priming between GSC and their isogenic differentiated counterparts. To this end, bulk RNA sequencing data from E2, G7 GSC and their DIFF counterparts was analysed (30). Consistent with enrichment of GSC, RNAseq analysis revealed increased levels of CD34, a surface glycoprotein, first described as marker for haematopoietic progenitor cells (40). Interestingly, high expression of *NTRK2* mRNA was detected in both GSC (**Figure 4A**). This finding was validated in E2 and G7 GSC as well as R15 and R24 GSC via immunoblotting (**Figure 4B, Supplementary Figure 4A**). *NTRK2* the gene coding for the tropomycin receptor kinase B (TrkB) is primarily known for its function in neurodevelopment inducing downstream signalling upon binding of brain-derived neurotrophic factor (BDNF) (41). Recently, Wang and colleagues have reported a role for TrkB-expressing cancer stem cells in GBM progression in response to BDNF stimulation by

differentiated tumour cells (42). As TrkB-mediated activation of MAPK and PI3K-AKT signalling is generally associated with cell survival (43), we hypothesised that BDNF-mediated TrkB stimulation might enable GSC to evade cell death. Unexpectedly, following stimulation of GSC with BDNF or 7,8-dihydroxyflavone (7,8-DHF), a specific TrkB agonist, we found that GSC were further sensitised to cell death following treatment with BH3-mimetics targeting BCL-xL and or MCL-1 (**Figure 4C, Supplementary Figure 4B**). This sensitising effect was not observed in the DIFF cells (**Figure 4D**). DIFF cells express significantly lower levels of the TrkB receptor and therefore prove to be comparably unresponsive to BDNF stimulation (**Supplementary Figure 4C**). BDNF-induced TrkB phosphorylation also led to increased BCL-xL protein expression, alongside stabilisation of the BIM protein downstream of MAPK signalling, independently of BCL-xL and MCL-1 inhibition (**Figure 4E**). These data demonstrate a key role for BDNF-TrkB signalling in the increased apoptotic priming of GSCs.

Combined BCL-xL and MCL-1 inhibition causes apoptosis in human GBM ex vivo

Current *in vitro* methodologies fail to recapitulate important aspects of the brain microenvironment and tissue context. Given this, we sought to use a more physiologically relevant model to investigate functional responses to BCL-xL and MCL-1 inhibition in GBM. For this purpose, we developed an assay tailored to the use of freshly resected human GBM to be cultured *ex vivo* as tissue slices that could be readily exposed to candidate drugs (experimental setup illustrated in **Supplementary Figure 5A**). All three patients included in the study were diagnosed with *IDHwt* GBM. Tissue slices were treated for 72 hours in total. In all cases, we found that a combined therapy with A-1331852 and S63845 (BCL-xL and MCL-1 inhibition) significantly reduced tumour cell count compared with single drug treatment or control (**Figure 5A-D, Supplementary Figure 5B-D**). Moreover, dual treatment induced a significant reduction of cell proliferation (Ki67 IHC) and amount of SOX2 positive tumour cells (**Figure 5E,F, Supplementary Figure 5E,F**), while Caspase 3 cleavage was increased. This data indicates that the dual treatment efficiently targets GBM stem-like cells

ex vivo. Importantly, the integrity of the brain tissue and vasculature was maintained (**Supplementary Figure 5G**).

In recent years, selective MCL-1 and BCL-xL inhibitors have been developed that show effective *in vivo* potency (31, 32). However, systemic exposure to both inhibitors is limited due to its combined toxicity (44). Because the blood-brain-barrier is only permissible to certain drugs, local or intrathecal drug application (45) might allow to circumvent systemic side effects in a clinical setting. To explore potential toxicities to resident brain cells, we obtained brain slices from 11-week old adult mice and exposed them to dual treatment with the indicated BH3-mimetics. In regions of the subventricular zone, an important neural stem cell niche, we detected only a moderate increase of cleaved Caspase 3 in a fraction of glial and neural progenitor cells (GFAP and NESTIN IF stain) (**Figure 5G,H**). In summary, these data suggest that dual targeting of BCL-xL and MCL-1 may provide a novel therapeutic approach to treat GBM.

Priming with BCL-xL inhibition renders GSC vulnerable to MCL-1 inhibition, promoting tumour regression in vivo

Given the potency of joint BCL-xL/MCL-1 inhibition in our *in vitro* and *ex vivo* findings, we sought to maximise this combinatorial effect whilst mitigating possible systemic toxicity. To address this, we investigated which pro-apoptotic proteins are involved in regulating intrinsic apoptosis in GBM. Upon single agent treatment with A-1331852, we observed upregulation of the BH3-only protein BIM as well as anti-apoptotic MCL-1. This was seen in both control and BAX/BAK deficient GSC (**Figure 6A**). BIM is an important BH3-only protein in the canonical apoptotic pathway where it functions by regulating both BCL-xL and MCL-1 mediated cell death responses (46). We hypothesised that MCL-1 might bind and neutralise BIM that is released by the A-1331852 complexing to BCL-xL. Accordingly, immunoprecipitation of MCL-1 following treatment with A-1331852 revealed increased binding of BIM to MCL-1 (**Figure 6B**). To explore whether this mechanism could be therapeutically exploited, we questioned whether BCL-xL inhibition would render GSC more

sensitive to subsequent MCL-1 inhibition. GSC were treated with a BH3-mimetic targeting either BCL-xL or MCL-1 for up to 48 hours followed by a washout and 24 hours treatment pause. Subsequently the complementary inhibitor was applied for up to 48 hours. Whereas prior inhibition with MCL-1 inhibitor failed to sensitise the cells to BCL-xL inhibition, pre-treatment with the BCL-xL inhibitor substantially increased the susceptibility of GSC to subsequent MCL-1 inhibition (**Figure 6 C,D**). To further investigate the relevance of BIM in mediating apoptosis following BCL-xL and MCL-1 inhibition, we deleted BIM by CRISPR/Cas9 genome editing (**Supplementary Figure 6A**). Using IncuCyte live cell imaging and Sytox Green exclusion to detect cell death under treatment we observed that knockout of BIM did not impede the sensitivity of G7 GSC to concurrent dual BCL-xL and MCL-1 inhibition (**Supplementary Figure 6B**). However, after pre-treatment with BCL-xL inhibitor A-1331852 G7 BIM^{CRISPR} GSC were less primed for following MCL-1 inhibition compared to their $vector^{CRISPR}$ counterparts (**Figure 6E**). These results indicate that Bcl-xL-inhibition mediates sensitisation of GSC to subsequent MCL-1 neutralisation via pro-apoptotic BIM.

Finally, we aimed to investigate the potency of alternating BH3-mimetic treatments in GBM *in vivo*. Due to the poor blood-brain-barrier penetrance of ABT-263, we chose a subcutaneous model. As the GSC used in our study do not grow as subcutaneous xenografts we explored whether human U87MG respond to combined and alternating inhibition of BCL-xL and MCL-1 in like manner to GSC. Indeed, we found that dual inhibition of BCL-xL and MCL-1 induced substantial cell death in U87MG neurospheres (**Supplementary Figure 6C**). Testing different treatment regimens using a clonogenic survival assay, we found a profound decrease in colony formation upon alternating treatment with ABT-263 and S63845 (**Supplementary Figure 6D**). In our *in vivo* cohort, mice were treated with vehicle or alternating therapy with ABT-263 and S63845 every 48 hours for two weeks upon tumour establishment (treatment schematic illustrated in **Supplementary Figure 6E**). Compared to mice receiving vehicle control, mice treated with the sequential therapy showed significant attenuation and/or regression of tumours (**Figure 6F**). Most

292 importantly, we observed significantly improved survival in mice treated with ABT-263,
293 followed by S63845 (**Figure 6G**). One mouse had a complete tumour regression after
294 sequential treatment with no reoccurrence of the subcutaneous tumour over an 8-week
295 follow up period. With this treatment schedule no significant weight loss (**Supplementary**
296 **Figure 6F**) or signs of neurological deficits were detected in mice. Histopathological analysis
297 of tumours reaching clinical end point showed a higher prevalence of a large central necrotic
298 areas in within the treatment cohort compared to vehicle control (83% vs. 33%)
299 (**Supplementary Figure 6G**). Collectively, these data demonstrate the therapeutic potential
300 of sequential BCL-xL and MCL-1 inhibition in GBM.

Discussion

Largely due to a dearth of effective treatment options, GBM patients have a dismal prognosis (37). Addressing this, we investigated the therapeutic potential of targeting anti-apoptotic BCL-2 proteins in GBM. Our analysis revealed high expression of anti-apoptotic BCL-xL and MCL-1 in GBM. Moreover, we also observed increased expression of BCL-xL and MCL-1 in GBM stem-like cells - a population of cells that are key for GBM development and treatment resistance *in vivo* (5, 6). Rather than promoting apoptotic resistance, elevated anti-apoptotic BCL-xL and MCL-1 expression in GSC compared to isogenic DIFF correlated with increased susceptibility to targeted inhibition using BH3-mimetics. This indicates that GSC are inherently primed for apoptosis. Exploiting this, we found that GBM were sensitive to BH3-mimetics targeting either MCL-1 or BCL-xL. Crucially, alternating dosing with BCL-xL followed by MCL-1 specific BH3-mimetics, led to durable treatment responses with preceding BCL-xL inhibition sensitising to MCL-1 inhibition *in vivo*. These data highlight the therapeutic potential of targeting BCL-xL and MCL-1 in GBM.

Recently, highly specific and potent BH3-mimetics have been developed to specifically target BCL-2, BCL-xL and MCL-1 (12, 31, 32). We used these to probe the individual dependencies of GBM in a panel of patient-derived GSC. Importantly, we found that GBM cells are largely dependent on BCL-xL or MCL-1 for survival, whereas BCL-2 plays a lesser role. Genetic deletion of *MCL-1* corroborated its key role in both promotion and maintenance of GBM. Consistent with our findings, indirect targeting of MCL-1 through CDK7 inhibition, causing transcriptional repression, sensitises GBM cell lines to ABT-263 (47). Further, we could demonstrate that both BCL-xL and MCL-1 are highly expressed, not only in GBM tumour cores, but also in GBM stem-like cells compared to their isogenic differentiated counterparts and astrocytes. The high expression and dependence of GBM on anti-apoptotic BCL-2 function is consistent with an increased state of apoptotic priming. As Sarosiek and colleagues have demonstrated, the tissue of origin plays a major role in determining the apoptotic sensitivity of a cell (28), therefore the high dependency of stem-like cells on BCL-

329 xL and MCL-1 might relate to their resemblance of cerebral precursor cells. Both anti-
330 apoptotic proteins play a major role in neurogenesis, while with brain maturation neurons
331 become refractory to apoptotic cell death (26, 28).
332
333 Unexpectedly, we observed that in comparison to their differentiated counterparts, stem-like
334 cells were more susceptible to BH3-mimetic treatment. Investigating the basis of the
335 differential apoptotic priming we identified NTRK2, a stem-cell specific surface receptor (42)
336 as a key component. NTRK2 signalling, mediated by the soluble brain derived neurotrophic
337 factor BDNF, plays a major role in cell survival promotion of growth in glial tumours (42, 48).
338 Surprisingly, we found that BDNF stimulation led to increased apoptotic priming. This result
339 reinforces the notion that stem-like cells are especially dependent on the tight regulation of
340 apoptotic sensitivity. More profound understanding of the tumour-environmental context
341 should shed light on how these interactions can be therapeutically exploited to maximise
342 treatment efficacy of BH3-mimetics.
343
344 To facilitate translation to the clinic, we developed an *ex vivo* assay to investigate
345 chemosensitivity of fresh patient derived GBM tissue to BCL-2 targeting BH3-mimetics.
346 Across different freshly resected *IDHwt* GBM samples, we found that targeting both MCL-1
347 and BCL-xL led to an extensive induction of apoptosis and sustained reduction in tumour cell
348 viability *ex vivo*, without compromising tissue and vessel integrity. Following inhibition of
349 BCL-xL we found an increased amount of BIM bound to MCL-1, leading to a sensitisation of
350 the GBM cells to MCL-1 antagonists. This mirrors studies in haematologic malignancies
351 where the susceptibility to BH3-mimetics was dependent on BCL-2 complexed to BIM (49,
352 50) and increased BIM levels sensitised to BCL-2 inhibition (51).
353
354 To circumvent reported systemic toxicity, we developed a sequential treatment schedule.
355 Our analysis of bioavailability in an orthotopic patient-derived xenograft revealed that the
356 blood-brain-barrier is barely penetrable for ABT-263. Using the GBM cell line U87MG in a

357 subcutaneous xenograft model, the observed effect of sequential priming could also be
358 recapitulated *in vivo* with a profound regression of tumour size and significant survival
359 benefit. Importantly, the brain, due to its blood-brain-barrier, provides unique opportunities
360 for drug delivery. For instance, local drug delivery or intrathecal chemotherapy can be
361 exerted to use the blood-brain-barrier and in turn circumvent systemic side effects (45). In
362 summary, these data provide a rationale for further investigating alternating inhibition of
363 BCL-xL and MCL-1 pro-survival function in GBM to maximise the therapeutic effect.
364

Materials and methods

Patient-derived GBM cell lines and cell culture reagents

Patient-derived GBM stem-like cells (E2, G1, G7, R9, R15, R24 GSC), obtained from surgical resection specimens of anonymised patients as described (52, 53), were kindly provided by Prof. Colin Watts. GSC and U87MG were cultured in serum-free Advanced Dulbecco's modified Eagle's medium F12 (Thermo Fisher Scientific), supplemented with 2mM glutamine, 4µg/ml heparin (Sigma), 1% B27 (Thermo Fisher Scientific), 0.5% N2 (Thermo Fisher Scientific), 20ng/ml EGF and 10ng/ml FGF (Thermo Fisher Scientific). DIFF cells were cultured in 10% foetal calf serum (FCS) containing high-glucose DMEM (Thermo Fisher Scientific) complemented with 2mM glutamine. Human astrocytes were originally provided by Prof. Steven Pollard as human foetal neural stem cells and previously differentiated to astrocytes by 7 days culture in differentiation inducing medium as described before (54). All cells were kept in 37°C incubator at 5% CO_2 and, when grown as monolayers on Matrigel (Corning) pre-coated plates or as spheres in uncoated plates. For all experiments, cells were used up to ten passages after thawing. All cell lines used were routinely tested for mycoplasma.

For our *in vitro* studies the following drugs and chemicals were used: ABT-199 (AdooQ BioScience, #A12500-50), ABT-263 (ApexBio, #A3007), ABT-737 (ApexBio, #A8193), A1331852 and A1155463 (ApexBio, #B6164 and #B6163), S63845 (Chemgood, #C-1370), Actinomycin D (Calbiochem, #114666), q-VD-OPh (QVD, AdooQ BioScience, #A14915-25), Sytox Green (Thermo Fisher Scientific, #S7020), Brain-derived neurotrophic factor (BDNF; Peprotech, #450-02), 7,8-Dihydroxyflavone hydrate (7,8-DHF; Merck, #D5446).

Lentiviral transduction

GSC transduction was performed using CRISPR/Cas9 genome editing with the following guide sequences:

hBAX: 5'-AGTAGAAAAGGGCGACAACC-3'

hBAK: 5'-GCCATGCTGGTAGACGTGTA-3'

393 *hMCL-1.1: 5'-GGGTAGTGACCCGTCCGTAC-3'*

394 *hMCL-1.2: 5'-GTATCACAGACGTTCTCGTA-3'*

395 *hBIM: 5'-* TACCCATTGCACTGAGATAG-*3'*

396 For stable cell line generation HEK293-FT cells ($4x10^6$ in a 10 cm dish) were transfected
397 using 4µg polyethylenimine (PEI, Polysciences) per µg plasmid DNA with the
398 LentiCRISPRv2-puro (Addgene #52961) or LentiCRISPRv2-blasti (55) backbone, lentiviral
399 transfer vector plasmid, packaging plasmid (Addgene #14887) and envelope plasmid
400 pUVSVG (Addgene #8454), mixed in a 4:2:1 ratio. DNA/PEI mixtures were incubated at
401 room temperature for 10 to 15 minutes, prior to application on HEK293-FTs. 24 and 48
402 hours later, virus containing supernatant was harvested and filtered (0.45µM). Virus was
403 extracted using Lenti-X concentrator (Clontech Takara) according to the manufacturer's
404 instructions. The virus containing pellet was resuspended in serum-free stem-cell medium
405 and target cells were infected in the presence of 1µg/ml polybrene (Sigma Aldrich). Two
406 days following infection, cells were selected by growth in puromycin (E2: 1µg/ml, G7:
407 0.5µg/ml; Sigma Aldrich) or blasticidin (G7, R15 and R24: 10 µg/ml; InvivoGen) containing
408 medium. As described previously, plasmids encoding iRFP IRES puro have been inserted
409 into a pBABE vector (36).
410
411 *Cell proliferation and live-cell viability assay*
412 Cell death and cell confluence were determined using live-cell imaging in the IncuCyte Zoom
413 and S3 (Sartorius). For cell confluence $50x10^3$ cells were seeded in Matrigel-coated 6-well
414 plates. Cell area per well was measured using IncuCyte imaging analysis software
415 (Sartorius). For cell death assays, $6x10^3$ or $12x10^3$ GSC per well were seeded in Matrigel-
416 coated 96-well plates and treated with the indicated drugs in the presence of 30nM SYTOX
417 Green. Plates were applied to the IncuCyte imager at 37°C in a humidified 95% air/ 5% CO_2
418 incubator. Every hour, two images per well were taken over a period of 24 to 48 hours.
419 Images were presented in green phase contrast at 10x magnification. For image
420 quantification IncuCyte imaging analysis software was used. Percentage cell death was

calculated by normalising against maximal cell death control upon 24 to 48 hours treatment (1μM Actinomycin D, 10μM ABT-737 and 1μM S63845). Alternatively, 100% cell death control was verified by visual inspection of IncuCyte images, where 100% Sytox Green positive cells = total cell count.

Clonogenic survival assay

GSC were seeded at a density of 250 cells per well in Matrigel-coated, 6-well plates with three technical repeats per experiment and left to adhere overnight. After 16 hours cells were treated as indicated for 24 hours, followed by replacement of fresh media. Cells were left to form colonies for 2 to 3 weeks prior to methanol fixation and crystal violet staining. Visible colonies consisting of minimum 50 cells were counted manually.

Neurosphere formation assay

G7 GSC vector^{CRISPR} and MCL-1^{CRISPR} were seeded at a density of 10 cells per well in uncoated 96-well plates. Serum-free stem-cell medium was refreshed every week. Spheres were left to grow for 14 days before manual scoring of the 60 inner wells.

Immunoblotting, immunoprecipitation and antibodies

GSC were lysed and collected in RIPA buffer (50mM Tris-HCl pH 7.5, 150 mM NaCl, 1 mM EDTA, 1% NP-40), supplemented with complete protease inhibitor (Roche) and PhosSTOP (Roche). Protein concentration was determined using Pierce BCA protein assay kit (Thermo Fisher Scientific) and protein lysates were subjected to electrophoresis through SDS–PAGE or 4-12% NuPage Bis-Tris protein gels (Thermo Fisher Scientific) followed by blotting onto nitrocellulose membranes. After blocking in 5% non-fat, dry milk or 2% BSA (Roche), membranes were probed with primary antibody (dilution 1:1000) BAK (Cell Signaling #12105), BAX (Cell Signaling #2772), BCL-2 (Cell Signaling #2762), BCL-xL (Cell Signaling #2762), MCL-1 (Cell Signaling #5453), BIM (Cell Signaling #2933), TrkB (Cell Signaling #4603), pTrkA (Tyr674/675)/pTrkB (Tyr706/707) (Cell Signaling #4621), ERK1/2 (Cell

Signaling #4695), pERK1/2 (Cell Signaling #4370), AKT (Cell Signaling #9272), pAKT (Ser473; Cell Signaling #4066), Caspase 3 (Cell Signaling #9662), cleaved Caspase 3 (Cell Signaling #9664), PARP1 (Cell Signaling #9532) and SOX2 (Abcam #ab92494), NESTIN (Abcam #ab22035), GFAP (Santa Cruz #SC-6170) at 4°C overnight in blocking buffer. α-tubulin (Sigma #T5168, 1:5000), β-tubulin (Cell Signaling #2146, 1:5000), HSP60 (Cell Signaling #4870, 1:1000), or actin (Sigma #A4700, 1:5000) served as loading controls. Each blot was probed with primary antibodies and a loading control. Representative loading controls are shown in figures. Membranes were incubated with Li-Cor secondary antibodies (IRDye 680RD donkey anti-mouse, IRDye 800CW donkey anti-rabbit, IRDye 800CW donkey anti-goat) for 1 hour at room temperature.

For immunoprecipitation (IP), rabbit antibodies were coupled to magnetic beads conjugated to anti-rabbit IgG (Dynabeads Sheep anti-rabbit IgG, Invitrogen, #11203D). The buffer containing 200 mM NaCl, 75 mM Tris-HCl pH 7, 15 mM NaF, 1.5 mM Na3VO4, 7.5 mM EDTA, 7.5 mM EGTA, 0.15% (v/v) Tween-20 and protein inhibitors (Thermo Fisher) were used to prepare cell lysates. Lysates were passed several times through a 26-gauge needle followed by centrifugation at 10,000g for 5 min at 4 °C. Lysates were added to the beads and rotated for 2 hours at 4 °C. After washes in Tween-20-containing buffer, lysates were analysed by immunoblotting.

Blots were imaged using Li-Cor Odyssey CLx (Li-Cor), acquired and processed using Image-Studio software (Li-Cor) and subsequently arranged using Adobe Illustrator.

Orthotopic intracranial and subcutaneous xenografts

All mouse experiments were carried out in accordance with the Animals Act 1986 (Scientific Procedures on living animals) and the regulatory guidelines of the EU Directive 2010 under project licences PPL P4A277133 and PP6345023 and ethical review (University of Glasgow). For intracranial xenograft 7-week old female CD1-nude mice (Charles River, UK) were orthotopically injected with 1 x 10^5 iRFP-labelled vector^{CRISPR} and MCL-1^{CRISPR} G7 GSC into the right striatum. Mice were monitored for the duration of the experiment and humanely

sacrificed when they showed neurological (hemiparesis, paraplegia) or general symptoms (hunched posture, reduced mobility, and/or weight loss >20%).

For subcutaneous xenograft 1 x 10^6 U87MG cells, previously cultured in stem-cell medium, were diluted in PBS and 50% growth factor reduced Matrigel and injected in the right flank of 8-week old female CD1-nude mice (Charles River, UK). For *in vivo* dosing, ABT-263 (ChemieTek #A263) was dissolved in 10% ethanol, 30% PEG glycol 400 and 60% Phosal 50 PG at 20 mg/kg and administered via oral gavage. S63845 (ChemieTek #S63845) was prepared in 2% vitamin E/d-α-tocopheryl polyethylene glycol 1000 succinate (Sigma) immediately prior to IV administration by tail vein injection at 25 mg/kg. Mice were treated with a 48-hours pause between drug administrations over a 14 days period. Tumour growth was monitored by caliper measurement three times per week and volume calculated using the equation ([length x width^2]/2). Clinical end point, at which mice were euthanised, was 15mm diameter or ulceration of the tumour.

Intravital cranial iRFP imaging and magnetic resonance imaging (MRI)

To examine intravital, intracranial tumour growth in animals bearing iRFP-positive G7 GSC, mice were monitored by PEARL imaging (Li-Cor) as previously described (36). MRI scans performed on brain tumour bearing mice using a nanoScan PET/MRI scanner (Mediso Medical Imaging Systems, Hungary). Mice were maintained under inhaled isoflurane anaesthesia (induction 5% v/v; maintenance 1.5 - 2.0% v/v) in the medical air during imaging procedure duration. Whole brain T2 Fast Spin Echo (FSE) 3D Axial Sequences (slice thickness 1.0 mm, repetition time (TR) 2000 msec, echo time (TE) 83.7 msec, Flip Angle 90 degrees) were used to acquire MRI scans. For assessments of scans, volume-of-interest (VOI) was manually drawn around the tumour region on MRI scans by visual inspection. Separate VOI were drawn for each scan to adjust for the position of the mice on the scanner and tumour size.

Patient-derived GBM specimens and tissue culture

GBM specimens were obtained from surplus tumour tissue resected from patients treated within the OPARATIC study (NCT01390571). Patients had consented for use of surplus tissue for future research projects.

Fresh GBM tissues were obtained from surplus surgical resection tissue from patients at the Queen Elizabeth University Hospital (QEUH) in Glasgow after review by neuropathology with appropriate consent and in accordance with the NHS GG&C ethical committee review (Biorepository Application No. 432). The patient study was conducted in accordance with the Declaration of Helsinki. Neuropathological diagnosis and selected patient information are displayed in the figures. Further, details of these patients are restricted by institutional requirements. All experiments were performed conform to relevant regulatory standards of the CRUK Beatson Institute. Fresh samples were attenuated in 2% low gelling temperature agarose (Merck) and cut into 350µm thick slices using the McIlwain tissue slicer (Campden Instruments). Tissue slices were dissected under the microscope in ice cold PBS before they were transferred on top of hydrophilic Millicell cell culture inserts (Merck Millipore) into serum-free Advanced Dulbecco's modified Eagle's medium F12 supplemented with 0.5% N2, 1% B27, 1% glutamine and 1% penicillin-streptomycin and left to equilibrate for 24 hours at 37°C in a humidified 95% air/ 5% CO_2 incubator, before treatment with indicated drugs for 72 hours. Following PBS washes brains were fixed in 4% paraformaldehyde (PFA) overnight.

Organotypic adult mouse brain slice culture

Extracted brains from three 11-week old C57BL/6J mice were transferred to sterile PBS on ice, divided into both hemispheres and cut into coronal, 100µm thick slices using a vibratome (Campden Instruments 5100mz, advance speed 1mm/sec, oscillation amplitude 1.5mm, 80Hz). Up to 5 slices per hemisphere were cut around the subventricular zone (SVZ). Slices were cultured on top of cell culture inserts in neurobasal medium as described in the previous section and left to equilibrate for 1 hour at 37°C in a humidified 95% air/ 5%

531 CO_2 incubator before treatment with indicated drugs for 24 hours. After PBS washes slices
532 were fixed in 4% PFA overnight.
533
534 *Immunohistochemistry (IHC) and immunofluorescence (IF)*
535 H&E staining and IHC was performed on 4µm formalin fixed paraffin embedded (FFPE)
536 sections. For BCL-xL (Cell Signalling #2764), cleaved Caspase 3 (Cell Signalling #9661)
537 and MCL-1 (Abcam # ab32087) IHC staining the Leica Bond Rx Autostainer was used. All
538 FFPE sections underwent on-board antigen retrieval for 20 minutes using ER2 retrieval
539 buffer (Leica, UK) before staining at a previously optimised dilution (BCL-xL 1:500; cleaved
540 Caspase 3 1:500; MCL-1 1:200) and visualised with Liquid DAB (Agilent, UK). Ki67 (Agilent
541 #M7240) staining was performed on a Dako Autostainer Link 48 using high pH TRS retrieval
542 buffer performed in a PT module (20 mins at 97°C). Ki67 was applied at 1:100 dilution
543 before visualising using Liquid DAB. For SOX2, IHC epitope retrieval was achieved by
544 heating to 98°C in pH6 citrate buffer for 60 minutes before proceeding as per the
545 manufacturer's instructions with SOX2 antibody used at a dilution of 1:500. Scanning and
546 image analysis was conducted using Halo (Indica Labs). Algorithms were optimised for each
547 stain individually and automated, quantitative analysis undertaken with Halo software (Indica
548 Labs).
549 For IF staining tissue slices were permeabilised and blocked in PBS with 10% NGS, 1%
550 BSA, 0.3% TX-100 and 0.05% Azide for 1 hour at room temperature. After washes with 10%
551 NGS, 1% BSA, 0.1% TX-100 and 0.05% Azide containing buffer slices were incubated with
552 primary antibodies (NESTIN 1:300, GFAP 1:400, cl. Caspase 3 1:400) in washing buffer for
553 72 hours at 4°C. After washes slices were incubated in secondary antibodies (1:200, Alexa
554 Fluor 568 goat anti-mouse (#A11004), Alexa Fluor 488 goat anti-rabbit (#A11034), Life
555 Technologies) in washing buffer for 24 hours. Following washes in PBS tissues were
556 counterstained with DAPI (VECTASHIELD, LSBio) and mounted in gaskets (BioRad Seal
557 Frame Incubation Chambers) on glass cover slips. Images were acquired using a Zeiss 710
558 laser scanning microscope with an EC Plan-Neofluar 40x/1.30 Oil DIC M27 objective and

559 Zen 2.3 SP1 FP3 (black edition) software. 70µm Z-stacks were acquired at 2.5µm intervals
560 and Maximum Intensity Projections (MIPs) were generated using Zen 2.1 (blue edition).
561 Image processing was performed using Fiji (ImageJ 1.53c). Cleaved Caspase 3 positive
562 cells were counted manually and nuclei were counted automatically using CellProfiler
563 (Version 4.0.7).
564
565 *In silico and transcriptomic analysis*
566 REMBRANDT microarray data was obtained from gliovis.bioinfo.cnio.es. Data was filtered
567 for histology and tumour grading.
568 RNA sequencing data was obtained from a previously published GBM database (30). In
569 order to determine the most differentially expressed genes, calculation of expression rank
570 product was employed to assess relative gene expression in paired GSC and DIFF cell lines
571 (56). Only results > 10 reads were incorporated.
572
573 *Statistical analyses*
574 For comparison of two experimental groups two tailed, unpaired *t* test with Welch's
575 correction (Welch's test) or Mann-Whitney test were used. For tumour related Kaplan–Meier
576 survival curves Mantel-Cox (Log-rank) was plotted. All statistical analyses were executed
577 with Prism software version 9 (GraphPad, La Jolla, CA, USA).
578
579
580 **Acknowledgements**
581 First and foremost, our special gratitude goes to the GBM patients who agreed to make their
582 tumour specimens available for research. Special thanks to Mary Fraser, Dr. Alexandru
583 Stan, Dr. Zoltan Hanzely and the Neuropathology Department of the QUEH in Glasgow, who
584 obtained patient consent and provided support with GBM tissue sampling. Further, we would
585 like to thank the Core Services at the Cancer Research UK Beatson Institute with particular
586 thanks to Gemma Thomson, David Strachan, the Biological Services Unit and Histology. We

thank Prof. Colin Watts for generous sharing of the patient-derived GBM cell lines, Prof. Steven Pollard and Rodrigo Gutierrez Quintana for providing the human astrocytes. Many thanks to Dr. Jayanthi Anand and Dr. Dimitris Athineos for their invaluable support with the animal work. Many thanks to members of the Tait laboratory for discussion and input, and Catherine Winchester for critical reading and assistance in the preparation of this manuscript. Figures were created with BioRender.com. **Funding:** This work was supported by CRUK core funding to the Beatson Institute (A17196) to C.N., (A17196/A31287) to N.R.P., (A22903) to K.M.R. and J.O'P., and (A18277) to J.C.N., a CRUK Programme Foundation Award (C40872/A20145) to S.W.T., CRUK Clinical Research Fellowship (A23220) to A.L.K., funding by the University of Glasgow to D.K. and A.J.C. and funding by the Beatson Cancer Charity and Cancer Research UK RadNet Centre Glasgow (A28803) to K.S.. L.M.-E. was funded by the by Erasmus+ Program and Short Research stay fellowship for trainees by Universitat Autònoma de Barcelona.

Author Contributions

A.L.K. and S.W.G.T. conceived the study, designed the work plan and wrote the manuscript. A.L.K. performed the majority of the experiments. D.K., L.M.-E., J.O'P. and F.J.B. acquired data and provided technical support. N.R.P. performed IF imaging and analysis. D.K., K.S., C.C., C.N. and G.M. provided assistance with the *in vivo* models and related imaging. K.K. and W.S. supervised and supported patient specimen collection. A.J.C. provided the RNAseq dataset. Y.E., D.K. and M.R.J. performed and supported data analysis. Expertise and critical input as well as review of the manuscript was given by K.J.C., G.I., K.B., A.J.C., K.M.R. and J.C.N.

Competing interests

K.J.C. is a recipient of a share in royalty payments paid to the Walter and Eliza Hall Institute of Medical Research in relation to venetoclax.

References

1. Louis DN, Perry A, Reifenberger G, von Deimling A, Figarella-Branger D, Cavenee WK, et al. The 2016 World Health Organization Classification of Tumors of the Central Nervous System: a summary. Acta Neuropathol. 2016;131(6):803-20.
2. Stupp R, Mason WP, van den Bent MJ, Weller M, Fisher B, Taphoorn MJ, et al. Radiotherapy plus concomitant and adjuvant temozolomide for glioblastoma. N Engl J Med. 2005;352(10):987-96.
3. Ostrom QT, Cioffi G, Gittleman H, Patil N, Waite K, Kruchko C, et al. CBTRUS Statistical Report: Primary Brain and Other Central Nervous System Tumors Diagnosed in the United States in 2012–2016. Neuro-Oncology. 2019;21(Supplement_5):v1-v100.
4. Weller M, Van Den Bent M, Preusser M, Le Rhun E, Tonn JC, Minniti G, et al. EANO guidelines on the diagnosis and treatment of diffuse gliomas of adulthood. Nature Reviews Clinical Oncology. 2020.
5. Chen J, McKay RM, Parada LF. Malignant glioma: lessons from genomics, mouse models, and stem cells. Cell. 2012;149(1):36-47.
6. Bao S, Wu Q, McLendon RE, Hao Y, Shi Q, Hjelmeland AB, et al. Glioma stem cells promote radioresistance by preferential activation of the DNA damage response. Nature. 2006;444(7120):756-60.
7. Tait SW, Green DR. Mitochondrial regulation of cell death. Cold Spring Harb Perspect Biol. 2013;5(9).
8. Bock FJ, Tait SWG. Mitochondria as multifaceted regulators of cell death. Nature Reviews Molecular Cell Biology. 2020;21(2):85-100.
9. Campbell KJ, Tait SWG. Targeting BCL-2 regulated apoptosis in cancer. Open Biol. 2018;8(5).
10. Montero J, Gstalder C, Kim DJ, Sadowicz D, Miles W, Manos M, et al. Destabilization of NOXA mRNA as a common resistance mechanism to targeted therapies. Nature Communications. 2019;10(1).
11. Chonghaile TN, Sarosiek KA, Vo TT, Ryan JA, Tammareddi A, Moore VDG, et al. Pretreatment Mitochondrial Priming Correlates with Clinical Response to Cytotoxic Chemotherapy. Science. 2011;334(6059):1129-33.
12. Souers AJ, Leverson JD, Boghaert ER, Ackler SL, Catron ND, Chen J, et al. ABT-199, a potent and selective BCL-2 inhibitor, achieves antitumor activity while sparing platelets. Nature Medicine. 2013;19(2):202-8.
13. Roberts AW, Davids MS, Pagel JM, Kahl BS, Puvvada SD, Gerecitano JF, et al. Targeting BCL2 with Venetoclax in Relapsed Chronic Lymphocytic Leukemia. New England Journal of Medicine. 2016;374(4):311-22.
14. Wei AH, Strickland SA, Jr., Hou JZ, Fiedler W, Lin TL, Walter RB, et al. Venetoclax Combined With Low-Dose Cytarabine for Previously Untreated Patients With Acute Myeloid Leukemia: Results From a Phase Ib/II Study. J Clin Oncol. 2019;37(15):1277-84.
15. Dinardo CD, Pratz KW, Letai A, Jonas BA, Wei AH, Thirman M, et al. Safety and preliminary efficacy of venetoclax with decitabine or azacitidine in elderly patients with previously untreated acute myeloid leukaemia: a non-randomised, open-label, phase 1b study. The Lancet Oncology. 2018;19(2):216-28.
16. Lok SW, Whittle JR, Vaillant F, Teh CE, Lo LL, Policheni AN, et al. A Phase Ib Dose-Escalation and Expansion Study of the BCL2 Inhibitor Venetoclax Combined with Tamoxifen in ER and BCL2–Positive Metastatic Breast Cancer. Cancer Discovery. 2019;9(3):354-69.
17. Nangia V, Siddiqui FM, Caenepeel S, Timonina D, Bilton SJ, Phan N, et al. Exploiting MCL1 Dependency with Combination MEK + MCL1 Inhibitors Leads to Induction of Apoptosis and Tumor Regression in KRAS-Mutant Non–Small Cell Lung Cancer. Cancer Discovery. 2018;8(12):1598-613.
18. Wroblewski D, Mijatov B, Mohana-Kumaran N, Lai F, Gallagher SJ, Haass NK, et al. The BH3-mimetic ABT-737 sensitizes human melanoma cells to apoptosis induced by selective BRAF inhibitors but does not reverse acquired resistance. 2013;34(2):237-47.

669 19. Serasinghe MN, Missert DJ, Asciolla JJ, Podgrabinska S, Wieder SY, Izadmehr S, et
670 al. Anti-apoptotic BCL-2 proteins govern cellular outcome following B-RAFV600E inhibition
671 and can be targeted to reduce resistance. Oncogene. 2015;34(7):857-67.
672 20. Karpel-Massler G, Ishida CT, Bianchetti E, Zhang Y, Shu C, Tsujiuchi T, et al.
673 Induction of synthetic lethality in IDH1-mutated gliomas through inhibition of Bcl-xL. Nat
674 Commun. 2017;8(1):1067.
675 21. Tagscherer KE, Fassl A, Sinkovic T, Combs SE, Roth W. p53-dependent regulation
676 of Mcl-1 contributes to synergistic cell death by ionizing radiation and the Bcl-2/Bcl-XL
677 inhibitor ABT-737. Apoptosis. 2012;17(2):187-99.
678 22. Karpel-Massler G, Ishida CT, Bianchetti E, Shu C, Perez-Lorenzo R, Horst B, et al.
679 Inhibition of Mitochondrial Matrix Chaperones and Antiapoptotic Bcl-2 Family Proteins
680 Empower Antitumor Therapeutic Responses. Cancer Res. 2017;77(13):3513-26.
681 23. Lathia JD, Mack SC, Mulkearns-Hubert EE, Valentim CLL, Rich JN. Cancer stem
682 cells in glioblastoma. Genes & Development. 2015;29(12):1203-17.
683 24. Couturier CP, Ayyadhury S, Le PU, Nadaf J, Monlong J, Riva G, et al. Single-cell
684 RNA-seq reveals that glioblastoma recapitulates a normal neurodevelopmental hierarchy.
685 Nature Communications. 2020;11(1).
686 25. Reya T, Morrison SJ, Clarke MF, Weissman IL. Stem cells, cancer, and cancer stem
687 cells. Nature. 2001;414(6859):105-11.
688 26. Fogarty LC, Flemmer RT, Geizer BA, Licursi M, Karunanithy A, Opferman JT, et al.
689 Mcl-1 and Bcl-xL are essential for survival of the developing nervous system. Cell Death &
690 Differentiation. 2019;26(8):1501-15.
691 27. Opferman JT, Kothari A. Anti-apoptotic BCL-2 family members in development. Cell
692 Death & Differentiation. 2018;25(1):37-45.
693 28. Sarosiek KA, Fraser C, Muthalagu N, Bhola PD, Chang W, McBrayer SK, et al.
694 Developmental Regulation of Mitochondrial Apoptosis by c-Myc Governs Age- and Tissue-
695 Specific Sensitivity to Cancer Therapeutics. Cancer Cell. 2017;31(1):142-56.
696 29. Pollard SM, Yoshikawa K, Clarke ID, Danovi D, Stricker S, Russell R, et al. Glioma
697 Stem Cell Lines Expanded in Adherent Culture Have Tumor-Specific Phenotypes and Are
698 Suitable for Chemical and Genetic Screens. Cell Stem Cell. 2009;4(6):568-80.
699 30. Carruthers RD, Ahmed SU, Ramachandran S, Strathdee K, Kurian KM, Hedley A, et
700 al. Replication Stress Drives Constitutive Activation of the DNA Damage Response and
701 Radioresistance in Glioblastoma Stem-like Cells. Cancer Research. 2018;78(17):5060-71.
702 31. Leverson JD, Phillips DC, Mitten MJ, Boghaert ER, Diaz D, Tahir SK, et al. Exploiting
703 selective BCL-2 family inhibitors to dissect cell survival dependencies and define improved
704 strategies for cancer therapy. Sci Transl Med. 2015;7(279):279ra40.
705 32. Kotschy A, Szlavik Z, Murray J, Davidson J, Maragno AL, Le Toumelin-Braizat G, et
706 al. The MCL1 inhibitor S63845 is tolerable and effective in diverse cancer models. Nature.
707 2016;538(7626):477-82.
708 33. Hemmati HD, Nakano I, Lazareff JA, Masterman-Smith M, Geschwind DH, Bronner-
709 Fraser M, et al. Cancerous stem cells can arise from pediatric brain tumors. Proceedings of
710 the National Academy of Sciences. 2003;100(25):15178-83.
711 34. Sofroniew MV, Vinters HV. Astrocytes: biology and pathology. Acta
712 Neuropathologica. 2010;119(1):7-35.
713 35. Fanfone D, Idbaih A, Mammi J, Gabut M, Ichim G. Profiling Anti-Apoptotic BCL-xL
714 Protein Expression in Glioblastoma Tumorspheres. Cancers. 2020;12(10):2853.
715 36. Koessinger AL, Koessinger D, Stevenson K, Cloix C, Mitchell L, Nixon C, et al.
716 Quantitative in vivo bioluminescence imaging of orthotopic patient-derived glioblastoma
717 xenografts. Scientific Reports. 2020;10(1).
718 37. Weller M, van den Bent M, Tonn JC, Stupp R, Preusser M, Cohen-Jonathan-Moyal
719 E, et al. European Association for Neuro-Oncology (EANO) guideline on the diagnosis and
720 treatment of adult astrocytic and oligodendroglial gliomas. Lancet Oncol. 2017;18(6):e315-
721 e29.

722 38. Ahmed SU, Carruthers R, Gilmour L, Yildirim S, Watts C, Chalmers AJ. Selective
723 Inhibition of Parallel DNA Damage Response Pathways Optimizes Radiosensitization of
724 Glioblastoma Stem-like Cells. Cancer Res. 2015;75(20):4416-28.
725 39. Auffinger B, Tobias AL, Han Y, Lee G, Guo D, Dey M, et al. Conversion of
726 differentiated cancer cells into cancer stem-like cells in a glioblastoma model after primary
727 chemotherapy. Cell Death & Differentiation. 2014;21(7):1119-31.
728 40. Sidney LE, Branch MJ, Dunphy SE, Dua HS, Hopkinson A. Concise Review:
729 Evidence for CD34 as a Common Marker for Diverse Progenitors. STEM CELLS.
730 2014;32(6):1380-9.
731 41. Park H, Poo M-M. Neurotrophin regulation of neural circuit development and
732 function. Nature Reviews Neuroscience. 2013;14(1):7-23.
733 42. Wang X, Prager BC, Wu Q, Kim LJY, Gimple RC, Shi Y, et al. Reciprocal Signaling
734 between Glioblastoma Stem Cells and Differentiated Tumor Cells Promotes Malignant
735 Progression. Cell Stem Cell. 2018;22(4):514-28.e5.
736 43. Minichiello L. TrkB signalling pathways in LTP and learning. Nature Reviews
737 Neuroscience. 2009;10(12):850-60.
738 44. Weeden CE, Ah-Cann C, Holik AZ, Pasquet J, Garnier JM, Merino D, et al. Dual
739 inhibition of BCL-XL and MCL-1 is required to induce tumour regression in lung squamous
740 cell carcinomas sensitive to FGFR inhibition. Oncogene. 2018;37(32):4475-88.
741 45. Oberoi RK, Parrish KE, Sio TT, Mittapalli RK, Elmquist WF, Sarkaria JN. Strategies
742 to improve delivery of anticancer drugs across the blood–brain barrier to treat glioblastoma.
743 Neuro-Oncology. 2016;18(1):27-36.
744 46. Adams JM, Cory S. The BCL-2 arbiters of apoptosis and their growing role as cancer
745 targets. Cell Death & Differentiation. 2018;25(1):27-36.
746 47. Shang E, Nguyen TTT, Shu C, Westhoff M-A, Karpel-Massler G, Siegelin MD.
747 Epigenetic Targeting of Mcl-1 Is Synthetically Lethal with Bcl-xL/Bcl-2 Inhibition in Model
748 Systems of Glioblastoma. Cancers. 2020;12(8):2137.
749 48. Ni J, Xie S, Ramkissoon SH, Luu V, Sun Y, Bandopadhayay P, et al. Tyrosine
750 receptor kinase B is a drug target in astrocytomas. Neuro-Oncology. 2017;19(1):22-30.
751 49. Del Gaizo Moore V, Brown JR, Certo M, Love TM, Novina CD, Letai A. Chronic
752 lymphocytic leukemia requires BCL2 to sequester prodeath BIM, explaining sensitivity to
753 BCL2 antagonist ABT-737. Journal of Clinical Investigation. 2007;117(1):112-21.
754 50. Del Gaizo Moore V, Schlis KD, Sallan SE, Armstrong SA, Letai A. BCL-2
755 dependence and ABT-737 sensitivity in acute lymphoblastic leukemia. Blood.
756 2008;111(4):2300-9.
757 51. Mérino D, Khaw SL, Glaser SP, Anderson DJ, Belmont LD, Wong C, et al. Bcl-2, Bcl-
758 x(L), and Bcl-w are not equivalent targets of ABT-737 and navitoclax (ABT-263) in lymphoid
759 and leukemic cells. Blood. 2012;119(24):5807-16.
760 52. Fael Al-Mayhani TM, Ball SL, Zhao JW, Fawcett J, Ichimura K, Collins PV, et al. An
761 efficient method for derivation and propagation of glioblastoma cell lines that conserves the
762 molecular profile of their original tumours. J Neurosci Methods. 2009;176(2):192-9.
763 53. Carruthers R, Ahmed SU, Strathdee K, Gomez-Roman N, Amoah-Buahin E, Watts
764 C, et al. Abrogation of radioresistance in glioblastoma stem-like cells by inhibition of ATM
765 kinase. Molecular Oncology. 2015;9(1):192-203.
766 54. Pollard SM. In Vitro Expansion of Fetal Neural Progenitors as Adherent Cell Lines.
767 Humana Press; 2013. p. 13-24.
768 55. Lopez J, Bessou M, Riley JS, Giampazolias E, Todt F, Rochegue T, et al. Mito-
769 priming as a method to engineer Bcl-2 addiction. Nat Commun. 2016;7:10538.
770 56. Breitling R, Armengaud P, Amtmann A, Herzyk P. Rank products: a simple, yet
771 powerful, new method to detect differentially regulated genes in replicated microarray
772 experiments. FEBS Letters. 2004;573(1-3):83-92.
773
774

Figure legends

Figure 1. High anti-apoptotic BCL-2 family protein expression correlates with increased BH3-mimetic sensitivity in GBM

(**A**) Schematic overview of BH3-mimetic drugs used and their respective targets (**B**) Panel of six GSC cell lines and the human primary GBM cell line U87MG were treated with indicated drugs for 24 to 48 hours and analysed for cell viability using an IncuCyte imager and SYTOX Green exclusion. Results are presented as heatmap. Percentage cell death was calculated by normalising against maximal cell death (treatment with 1μM Actinomycin D, 10μM ABT-737 and 1μM S6384), n=3 independent experiments per cell line. (**C**) Immunoblot of BCL-2 family proteins, cell-line specific neural stem cell marker SOX2 and astrocyte lineage differentiation marker GFAP in human astrocytes and patient-derived GSC. α-tubulin served as loading control. Representative image from n=3 independent experiments. (**D,E**) Matched tumour and margin specimens were obtained from three patients diagnosed with GBM and stained for haematoxylin and eosin (H&E), BCL-xL and MCL-1 IHC (representative images of one case shown). H-score (analysis of intracellular BCL-xL and MCL-1 expression) was determined using automated analysis with Halo. Error bars represent mean +/-SD (***p=0.0002, *p=0.0404) Welch's test. Further representative images in lower magnifications are shown in Supplementary Figure 1C.

Figure 2. Anti-apoptotic MCL-1 is required for the growth and survival of GBM

(**A**) Representative images of neurosphere growth from G7 GSC vector^{CRISPR} (upper panel), MCL-1.1^{CRISPR} (middle panel) MCL-1.2^{CRISPR} (lower panel), respectively. Quantification of neurosphere formation capacity by G7 GSC vector^{CRISPR} vs. MCL-1.1^{CRISPR} or MCL-1.2^{CRISPR}. Error bars represent mean +/-SD from n=4 independent experiments (p=0.8146, ns, nonsignificant) Welch's test. (**B**) Representative images of brain MRI scans (tumour indicated by red dashed line) next to corresponding pseudocolour representations of iRFP signal of mice bearing iRFP tagged G7 GSC vector^{CRISPR} (upper panel) and MCL-1.2^{CRISPR} (lower panel) xenografts, respectively. iRFP signal was detected by PEARL scans (700nm

803 channel) (1) at week 8 and (2) at week 20 (vector^{CRISPR}) or week 36 (MCL1^{CRISPR}) post
804 injection. (**C**) Quantification of time to 20% iRFP signal increase of G7 vector^{CRISPR} n=13 vs.
805 G7 MCL-1^{CRISPR} tumours n=19, compared to 4 weeks post injection (baseline signal). Error
806 bars represent mean +/-SD (**p=0.0013) Mann-Whitney test. (**D**) Kaplan-Meier survival
807 graph of mice with orthotopic xenografts of G7 GSC iRFP vector^{CRISPR} n=9 (median survival
808 87 days) vs. MCL-1^{CRISPR} tumours n=10 (median survival undefined) post tumour cell
809 implantation (p<0.0001) Log-rank (Mantel-Cox) test.
810
811 **Figure 3. GSC display increased apoptotic priming and can be effectively killed by**
812 **dual BCL-xL, MCL-1 inhibition**
813 (**A**) G7 and E2 GSC were treated with DMSO (ctrl), A-1331852 or ABT-737 as indicated for
814 16 or 24 hours, respectively, harvested and protein expression was analysed by
815 immunoblot. α-tubulin served as loading control. Representative image from n=3
816 independent experiments shown. (**B**) G7 or R24 GSC vector^{CRISPR} vs. MCL1.1^{CRISPR} and
817 MCL1.2^{CRISPR} were treated with A-1331852 for 24 hours and analysed for cell viability using
818 an IncuCyte imager and SYTOX Green exclusion. Percentage cell death was calculated by
819 normalising against maximal cell death verified by visual inspection. Error bars represent
820 mean +/-SEM from n=3 independent experiments. (G7: *p=0.0218, **p=0.002, ***p=0.0006)
821 (R24: **p=0.0028, ****p<0.0001) Welch's test. (**C**) E2, G1, G7, R24 GSC were treated with a
822 combination of A-1331852 and S63845 in indicated concentrations for 24 hours and
823 analysed for cell viability using an IncuCyte imager and SYTOX Green exclusion.
824 Percentage cell death was calculated by normalising against maximal cell death as
825 described in Figure 1B. Error bars represent mean +/-SEM from n=3 independent
826 experiments. (E2 **p=0.0021, G1 **p=0.0022, G7 **p=0.0016, R24 *p=0.0123) Welch's test.
827 (**D**) Clonogenic survival assay of G7 GSC iRFP treated with indicated drugs 16 hours after
828 plating 250 cells per well. Colonies counted manually after 14 days. Error bars represent
829 mean +/-SD from n=3 independent experiments (**p=0.0038) Welch's test. Representative
830 images of a replicate in one independent repeat scanned on LICOR imager. (**E**) E2 GSC

vector^{CRISPR} and BAK/BAX^{CRISPR} were treated as indicated for 2 hours, harvested and protein expression was analysed by immunoblot. HSP60 served as loading control. Representative image from n=3 independent experiments. (**F**) E2 and R15 GSC and paired DIFF cells were treated either with DMSO (grey) or a combination of A-1331852 and S63845 (both 0.1 μM) for 24 hours and analysed for cell viability using an IncuCyte imager and SYTOX Green exclusion. Error bars represent mean +/-SEM from n=3 independent experiments. Representative IncuCyte images 24 hours after treatment are shown.

Figure 4. TrkB signalling regulates sensitivity of GSC to anti-apoptotic treatment

(**A**) Most differentially expressed genes in RNAseq analysis of E2 and G7 GSC vs. E2 and G7 DIFF. *NTRK2* codes for TrkB. (**B**) Immunoblot of TrkB in E2 and G7 GSC compared with paired DIFF cells. α-tubulin served as loading control. Representative image from n=2 independent experiments. (**C**) E2 and G7 and GSC treated with BDNF (100ng/mL) or 7,8-DHF (20μg/mL) +/- A-1331852 1μM and S63845 1μM for 24 hours (after a 24-hour starvation period in 1% glutamine containing DMEM/F12) and analysed for cell viability using an IncuCyte imager and SYTOX Green exclusion. Error bars represent mean +/-SEM from one of n=3 independent experiments (E2 *p=0.0166, G7 ***p=0.008) Welch's test. (**D**) G7 DIFF treated as described in Figure 4C and analysed for cell viability using an IncuCyte imager and SYTOX Green exclusion. Error bars represent mean +/-SEM from n=3 independent experiments (ns, p=0.9284). (**E**) G7 GSC were treated with 7,8-DHF (20μg/mL) +/- A-1331852 1μM and S63845 1μM for 1 hour, harvested and protein expression was analysed by immunoblot. α-tubulin served as loading control. Representative image from n=3 independent experiments.

Figure 5. Combined BCL-xL and MCL-1 inhibition causes apoptosis in human GBM *ex vivo*

(**A**-**C**) Representative images of H&E, Ki67 and cleaved Caspase 3 IHC of three patients diagnosed with *IDHwt* GBM (case 1-3; ctrl=DMSO, dual treatment=A-1331852 1μM + S63845 1μM) (**D-F**) Quantification of cellularity, percentage Ki67 and SOX2 positive cells/total cell count in all three cases treated with the drugs described in (A-C) for 72 hours. Error bars represent mean +/-SEM (**p=0.0021) Welch's test. (**G**) Representative images of IF staining of GFAP, NESTIN (both red) and cleaved Caspase 3 (green) in the subventricular zone (SVZ) of mouse brain slices, cultured and treated with DMSO or a combination of ABT-263 5μM and S63845 2μM for 24 hours, counterstaining with DAPI (blue). (**H**) Quantification of cleaved Caspase 3 positive cells normalised to nuclear count in single mice. Single dots represent analysed images. Error bars represent median (mouse 1: p=0.9198, p=0.3086; mouse 2: p=0.149, p=0.2974; mouse 3: **p=0.0044, p=0.0593; ns, nonsignificant) Welch's test. Scale bars = 50μm.

Figure 6. Priming with BCL-xL inhibition renders GSC vulnerable to MCL-1 inhibition, promoting tumour regression *in vivo*

(**A**) E2 GSC vector^{CRISPR} and BAK/BAX^{CRISPR} were treated with DMSO (-), A-1331852 and S63845 as indicated for 24 hours, harvested and protein expression was analysed by immunoblot. Representative image from n=2 independent experiments. β-tubulin served as loading control. (**B**) Direct binding interactions between MCL-1 and BIM were immunoprecipitated and interacting proteins were detected by western blot in G7 GSC treated for 16 hours with A-1331852 (Input=total cell lysate, IP=immunoprecipitated fraction). Representative image from n=2 independent experiments. (**C**) G7 GSC were treated with DMSO, A-1331852 or S63852 1μM for 48 hours, followed by 24 hours drug washout with exchange to fresh medium and treatment with indicated drugs for 24 hours. For cell viability analysis, IncuCyte imager and SYTOX Green exclusion was used. Error bars represent mean +/-SEM from n=3 independent experiments, (**p=0.003) Welch's test. (**D**) E2 GSC were pre-treated with DMSO or A-1331852 1μM (#) for 24 hours, followed by 24 hours drug

884 washout with exchange to fresh medium and treatment with indicated drugs for 48 hours.
885 For cell viability analysis, IncuCyte imager and SYTOX Green exclusion was used. Error
886 bars represent mean +/-SEM from n=3 independent experiments, (***p=0.0004) Welch's
887 test. (**E**) G7 GSC vector^{CRISPR} and BIM^{CRISPR} were treated for 48 hours with A-1331852 1μM,
888 followed by 24 hours drug washout with exchange to fresh medium and treatment with
889 S63845 1μM for 24 hours. For cell viability analysis, IncuCyte imager and SYTOX Green
890 exclusion was used. Error bars represent mean +/-SEM from n=3 independent experiments,
891 (*p=0.0132) Welch's test. (**F**) Percent U87MG subcutaneous tumour volume change at the
892 end of 2 weeks alternating treatment with ABT-263, followed by S63845, relative to tumour
893 size at start. Treatment commenced when tumours were >5mm diameter. n=6 vehicle
894 treated (grey dots) and n=7 drug treated (blue dots). Bars are mean +/- SD (*p=0.0104)
895 Welch's test. (**G**) Kaplan-Meier survival analysis of U87 vehicle treated (grey line, n=6,
896 median survival 22 days) vs. U87 drug treated (blue line, n=7, median survival 34 days)
897 since treatment start (**p=0.0056) Log-rank (Mantel-Cox) test.
898

A

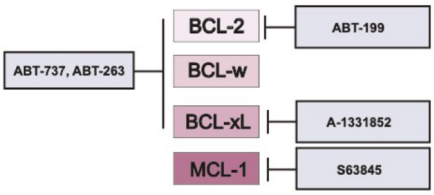

B

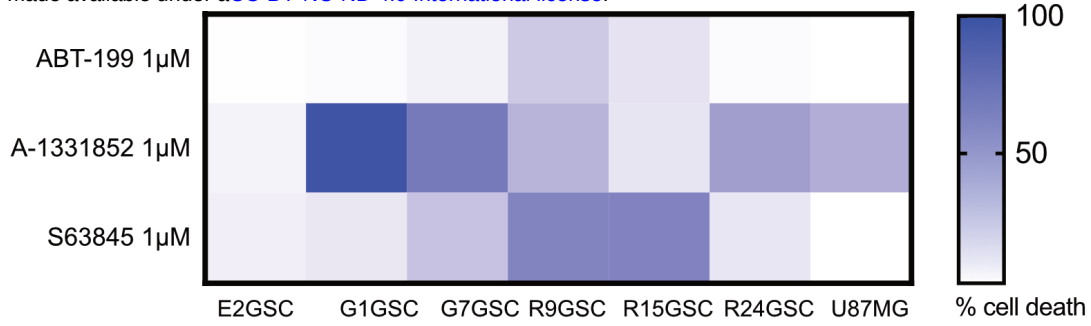

C

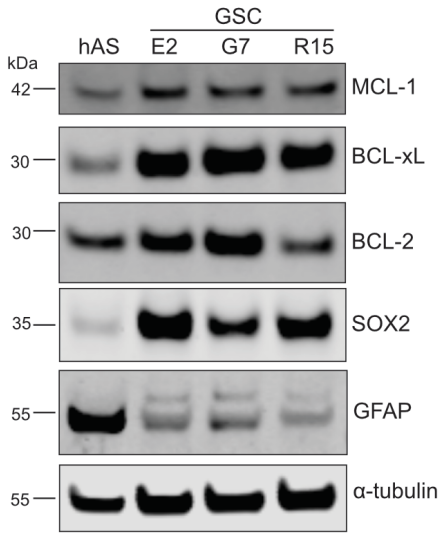

E

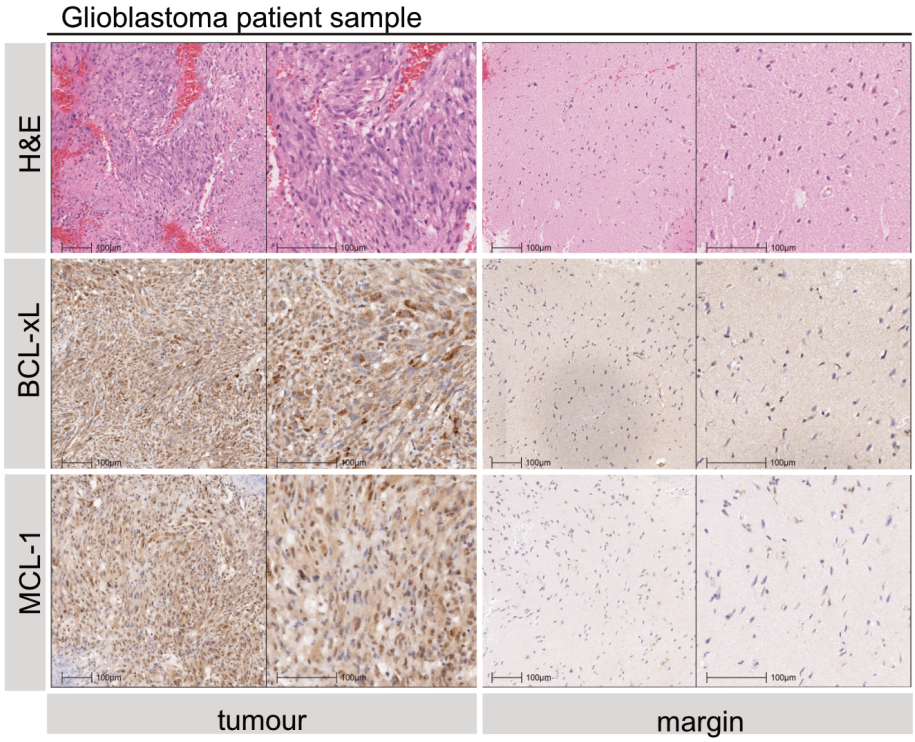

D

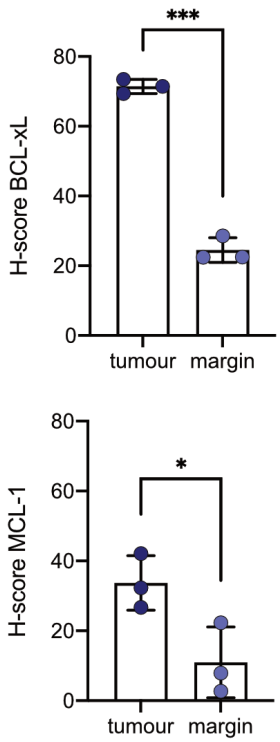

Figure 1

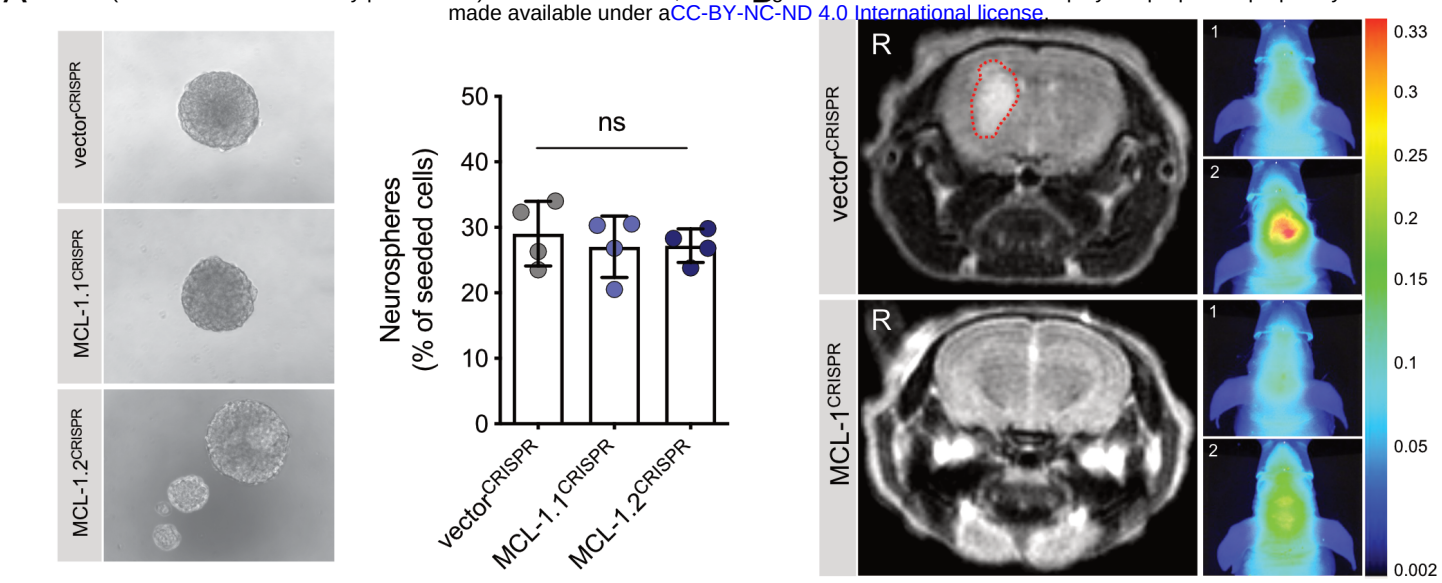

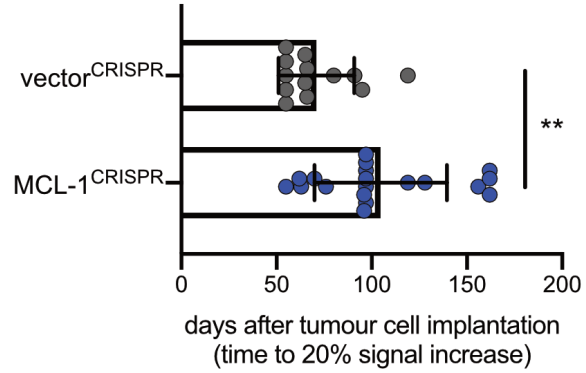

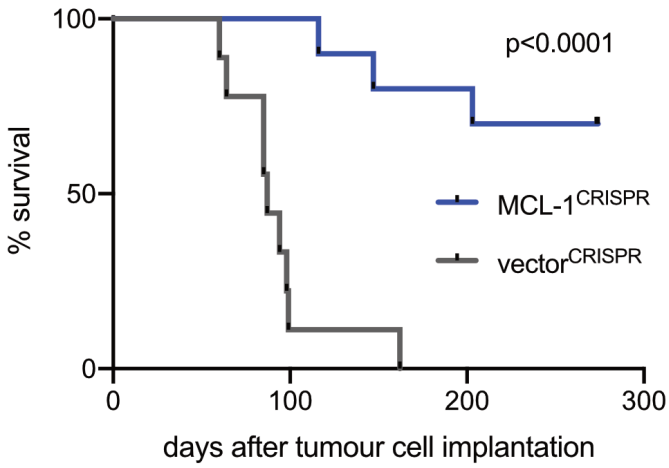

Figure 2

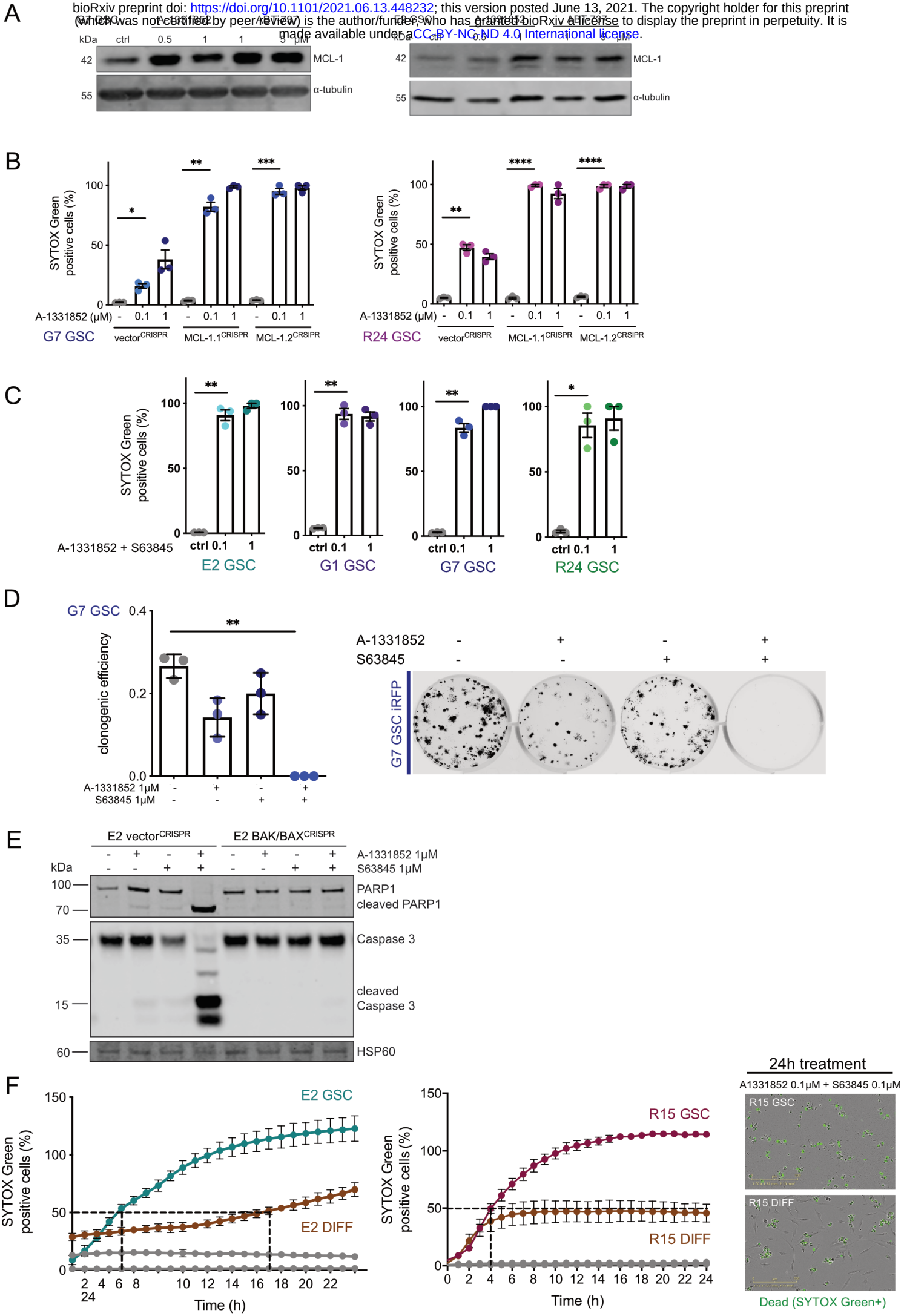

Figure 3

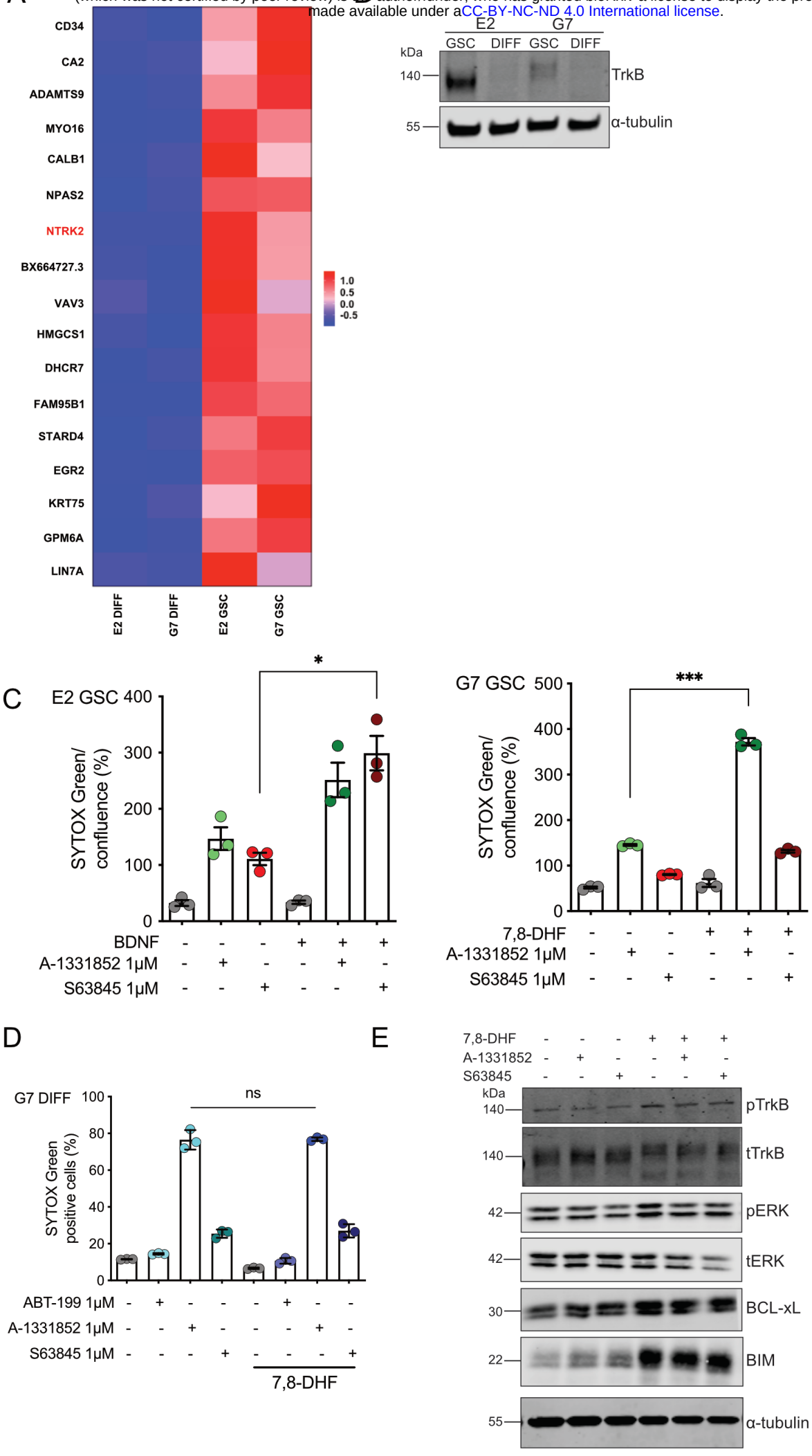

Figure 4

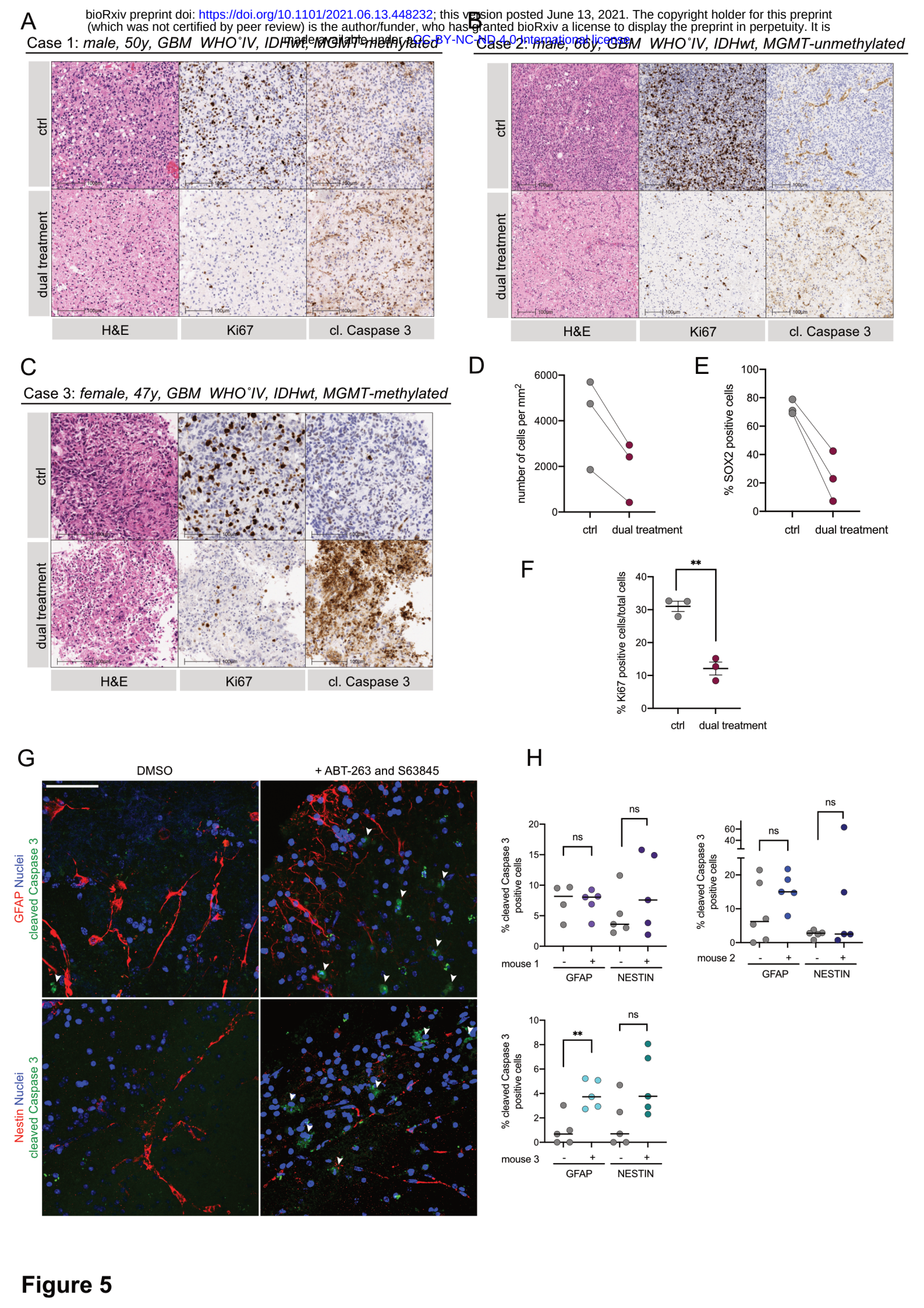

Figure 5

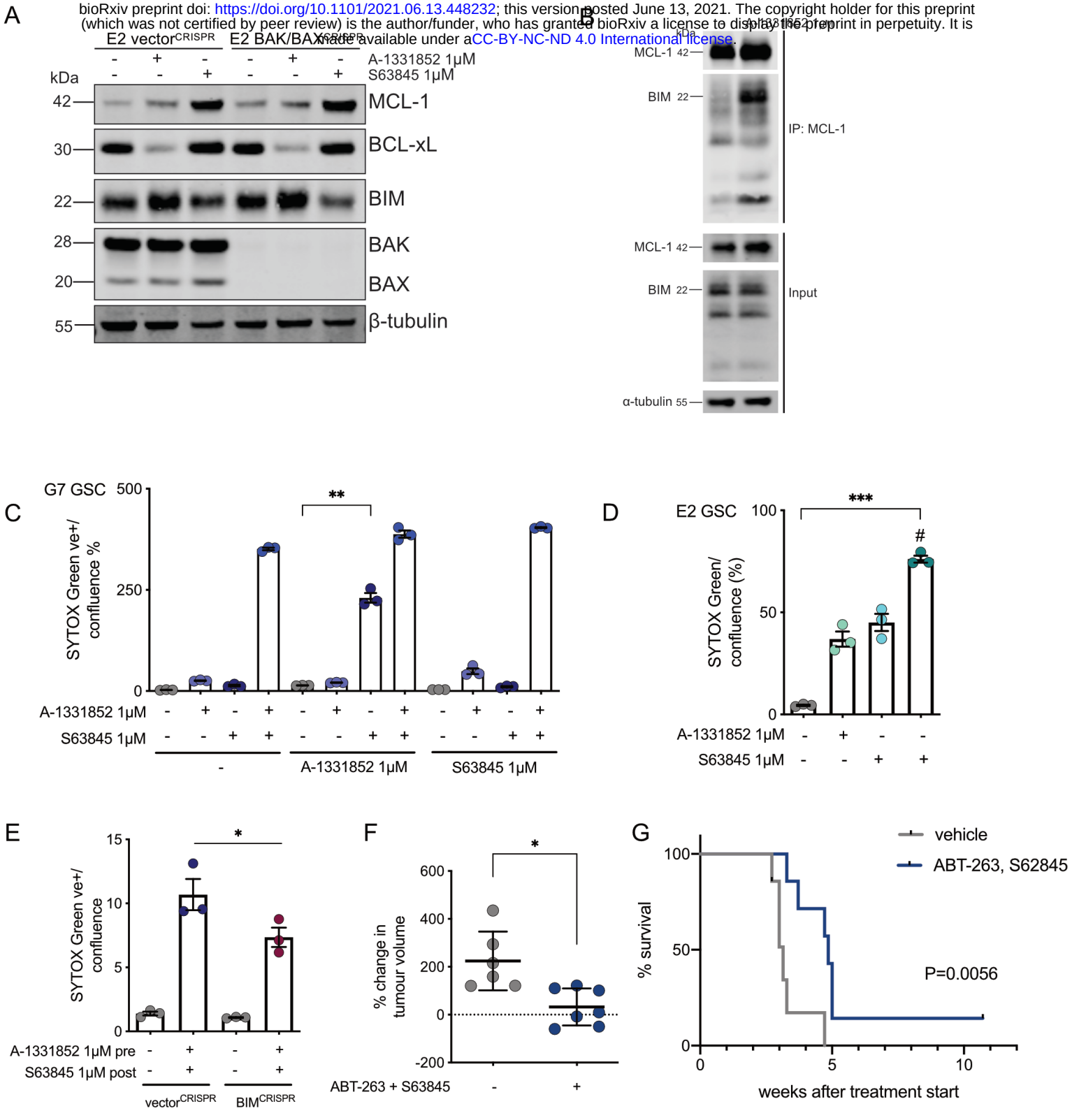

Figure 6

A

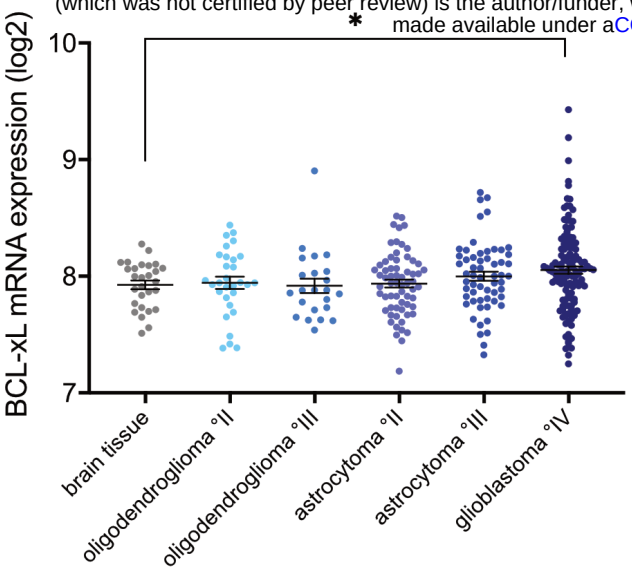

B

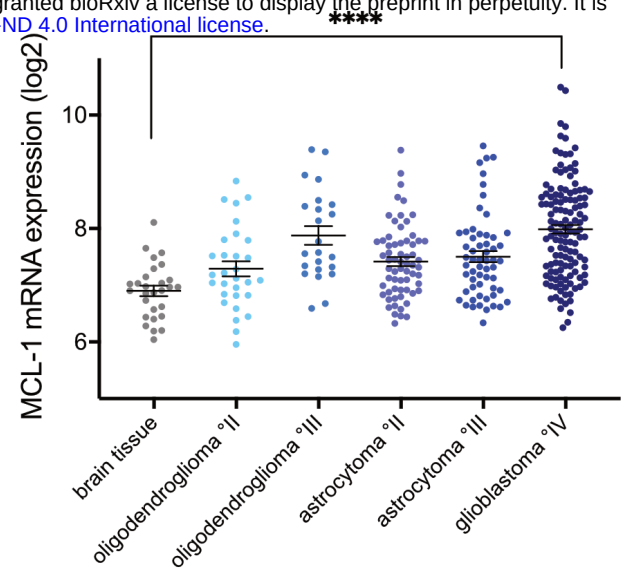

D

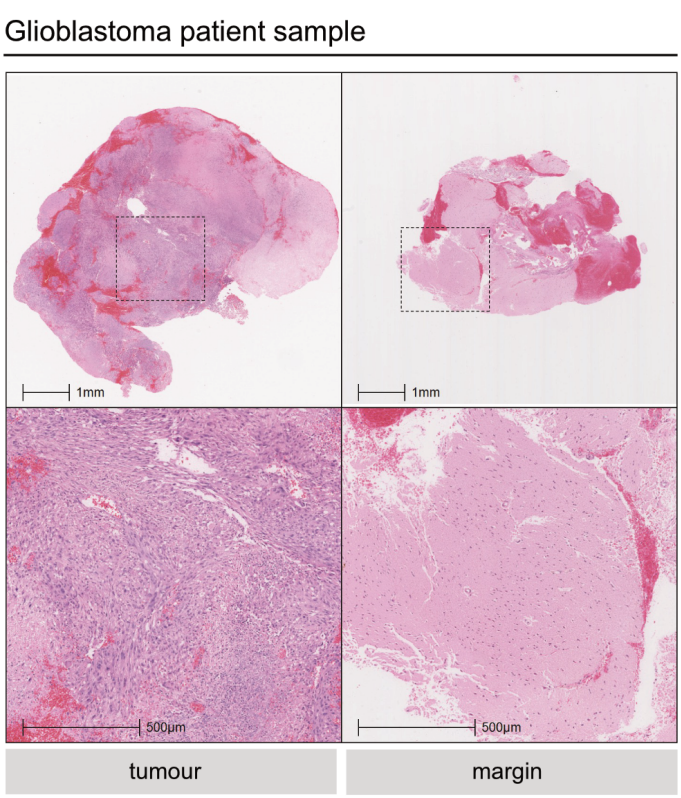

Supplementary data 1

A

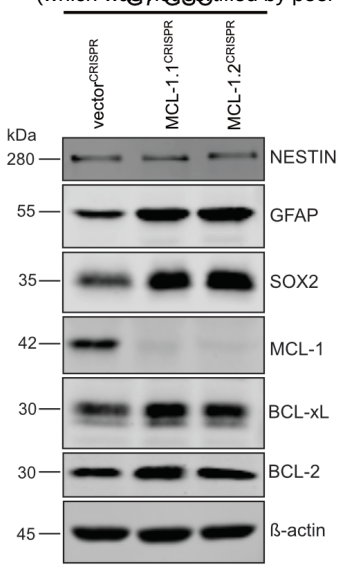

B

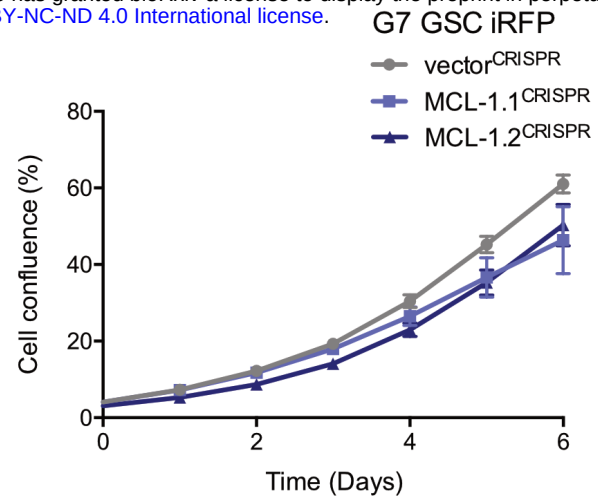

C

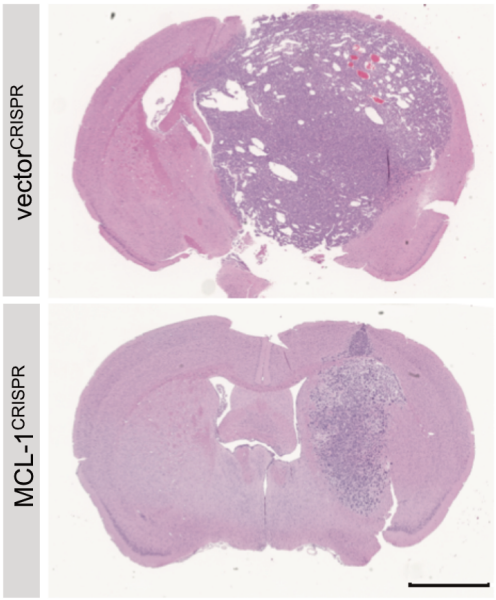

D

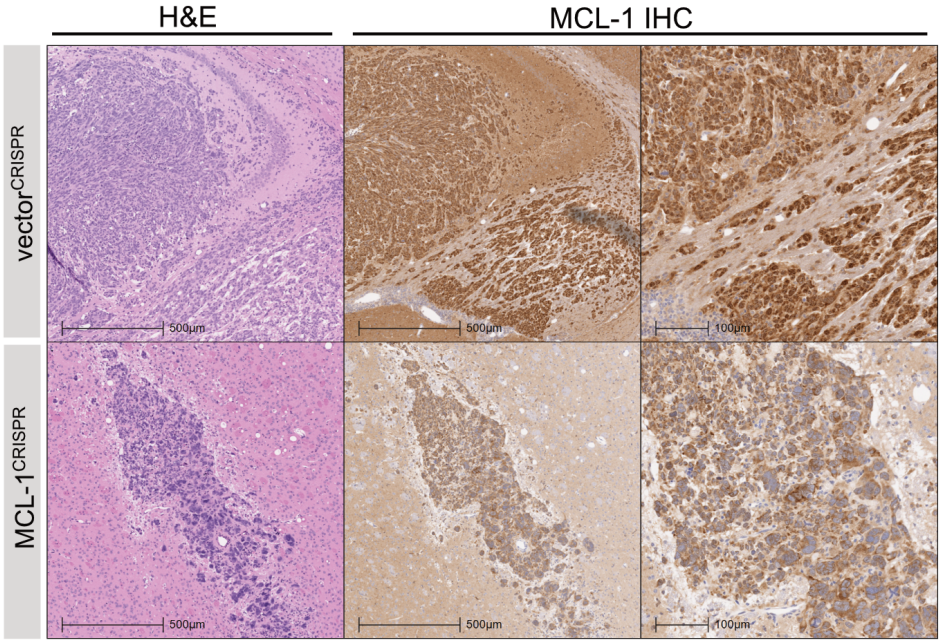

Supplementary data 2

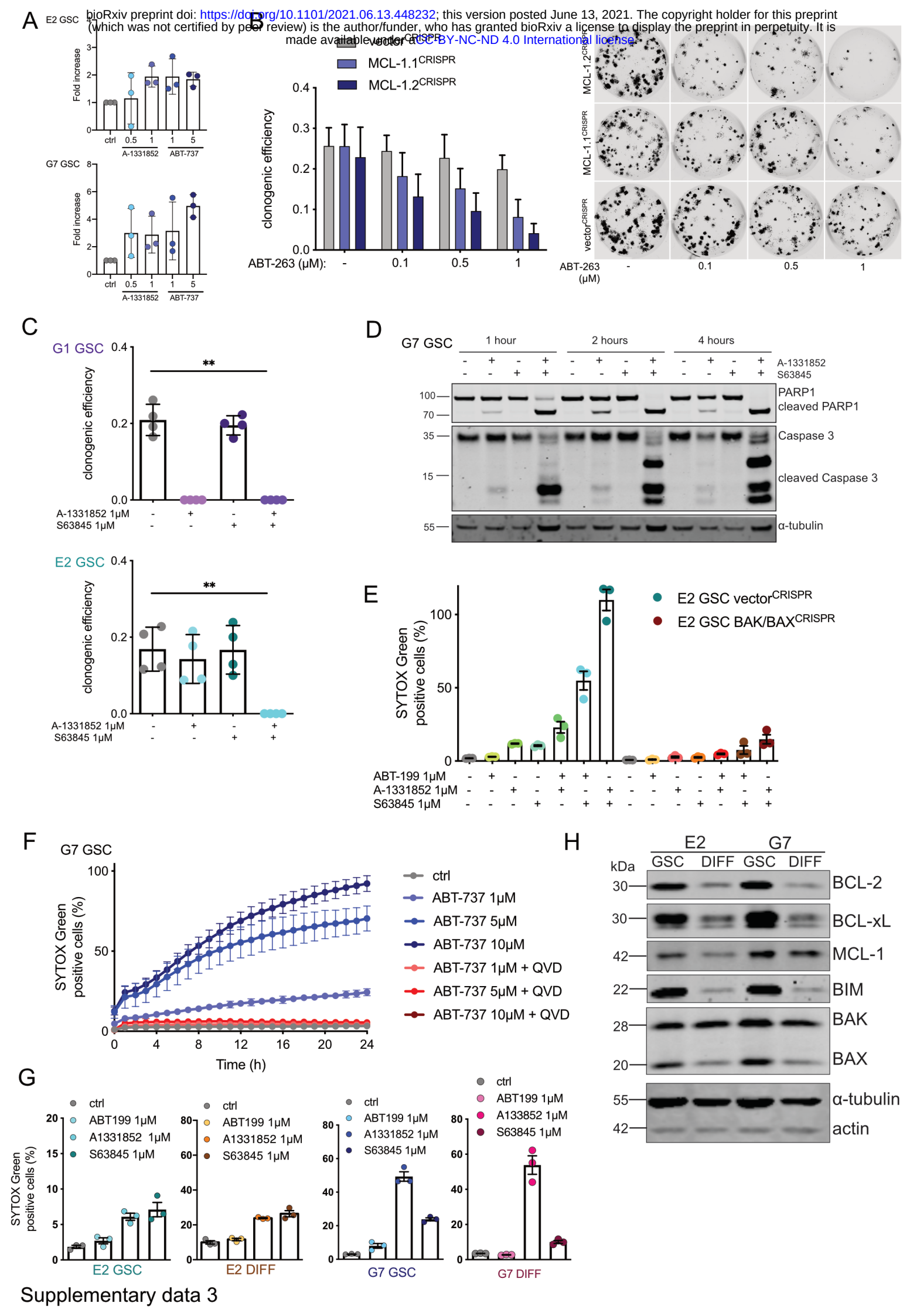

Supplementary data 3

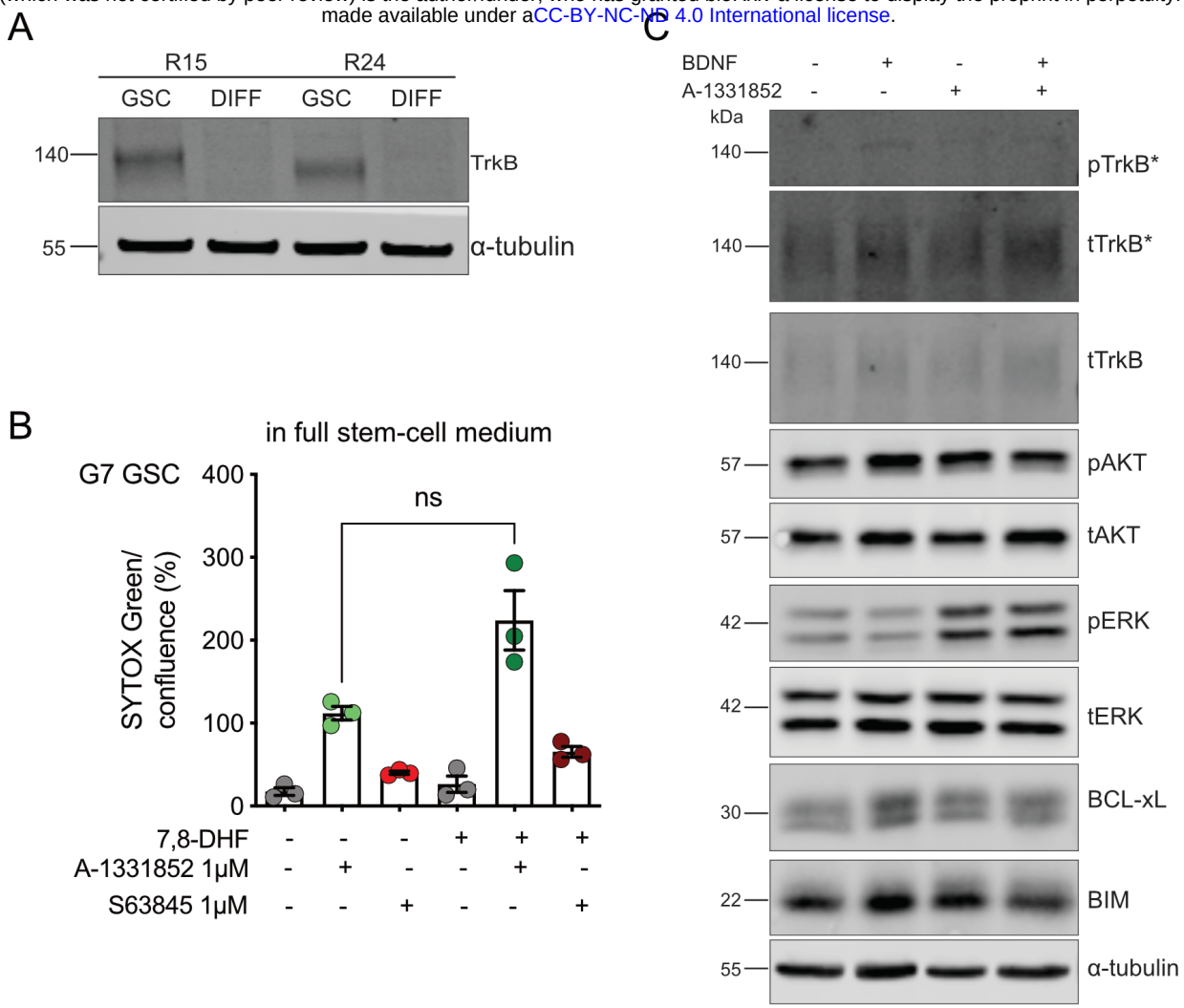

Supplementary data 4

A

B

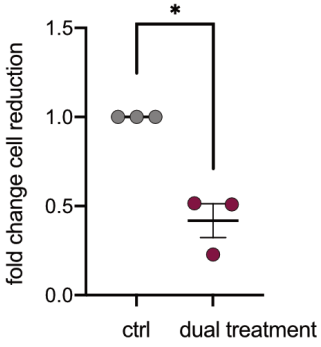

E

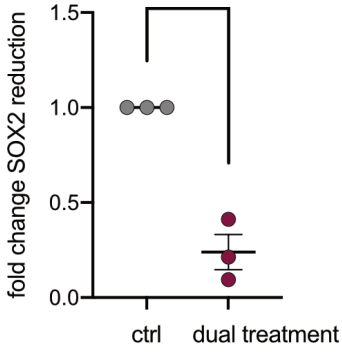

F

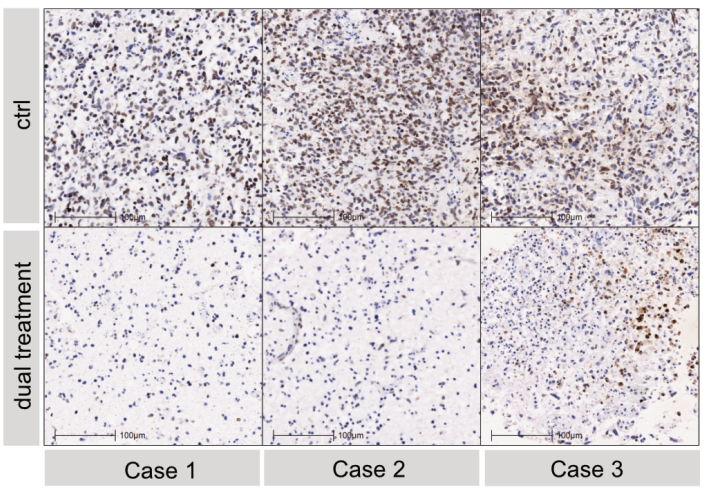

C

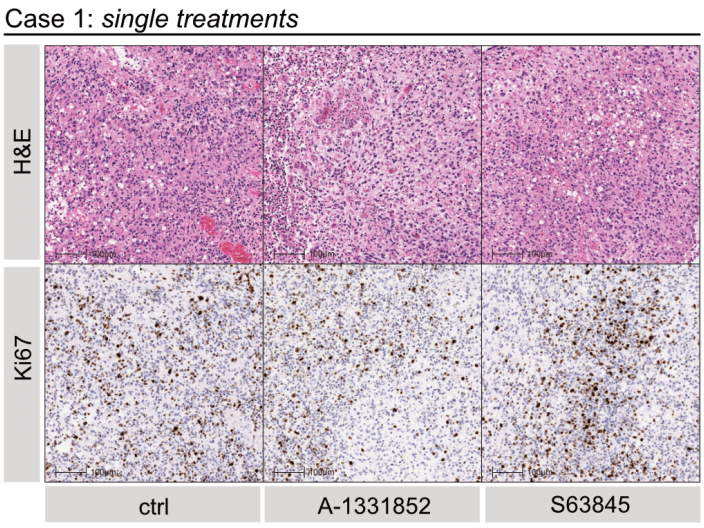

D

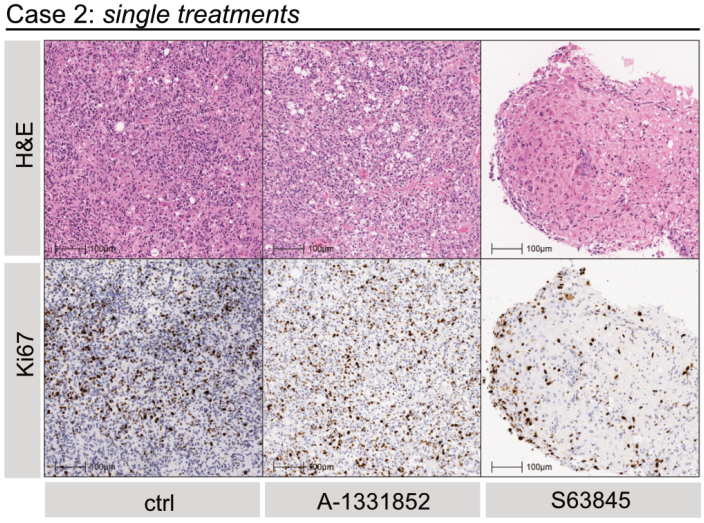

G

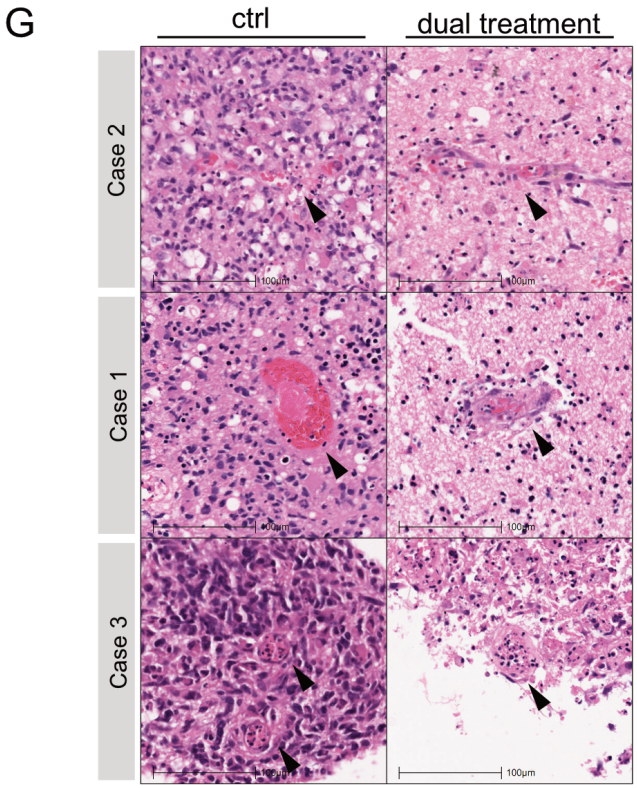

Supplementary data 5

Supplementary Figure legends

Supplementary Figure 1. Relevant to Figure 1.

(**A**,**B**) BCL-xL and MCL-1 mRNA expression from the publicly available REMBRANDT GBM microarray dataset. Data plotted for different glioma subtypes and normal brain tissue. Error bars represent mean +/-SEM (*p=0.0118, ****p<0.0001) Welch's test. (**C**) Corresponding representative H&E images of GBM tumour and margin samples shown in lower magnification than in Figure 1D.

Supplementary Figure 2. Relevant to Figure 2.

(**A**) Immunoblotting of G7 GSC vector^{CRISPR}, MCL1.1^{CRISPR} and MCL1.2^{CRISPR} for BCL-2 family proteins, cell-line specific neural stem cell marker (SOX2, NESTIN) and astrocyte lineage differentiation marker GFAP. Actin served as loading control. (**B**) Proliferation assay of indicated cell lines using IncuCyte Imager and – percentage cell density over 6 days. Error bars represent mean +/-SD from n=3 independent experiments. (**C**) Representative H&E images of G7 GSC iRFP vector^{CRISPR} and MCL1^{CRISPR} orthotopic xenografts at end point (corresponding to Figure 2B). Scale bar = 100μm. **(D)** Representative images of H&E and MCL-1 IHC of G7 GSC iRFP vector^{CRISPR} and MCL1^{CRISPR} orthotopic xenografts at end point.

Supplementary Figure 3. Relevant to Figure 3.

(**A**) Quantification of immunoblots shown in Figure 3A. (**B**) Clonogenic survival assay of G7 GSC iRFP vector^{CRISPR} vs. MCL1.1^{CRISPR} and MCL1.2^{CRISPR} treated with indicated drugs 16 hours after plating 250 cells per well. Colonies counted manually after 14 days. Error bars represent mean +/-SD from n=4 independent experiments. Representative images scanned on LICOR imager. (**C**) Clonogenic survival assay of E2 and G1 GSC iRFP treated with indicated drugs 16 hours after plating 250 cells per well. Colonies counted manually after 14 days. Error bars represent mean +/-SEM from n=4 independent experiments (E2**p=0.0099, G1**p=0.002) Welch's test. (**D**) G7 GSC were treated with DMSO (-), A-1331852 and

S63845 for indicated times, harvested and protein expression was analysed by immunoblot. α-tubulin served as loading control. Representative image from three independent experiments. (**E**) E2 GSC vector^{CRISPR} and BAK/BAX^{CRISPR} treated with indicated drugs for 48 hours and analysed for cell viability using an IncuCyte imager and SYTOX Green exclusion. Percentage cell death was calculated by normalising against maximal cell death as described in Figure 1B. Error bars represent mean +/-SEM from n=3 independent experiments. (**F**) G7 GSC treated with indicated drugs (+/-QVD 10μM) for 24 hours and analysed for cell viability using an IncuCyte imager and SYTOX Green exclusion. Percentage cell death was calculated by normalising against maximal cell death as described in Figure 1B. Error bars represent mean +/-SEM from n=3 independent experiments. (**G**) E2 and G7 GSC with paired DIFF cells treated with indicated drugs for 24 hours and analysed for cell viability using an IncuCyte imager and SYTOX Green exclusion. Percentage cell death was calculated by normalising against maximal cell death as described in Figure 1B. Error bars represent mean +/-SEM from n=3 independent experiments. (**H**) Immunoblot of E2 and G7 GSC with paired DIFF cells for BCL-2 family proteins. α-tubulin served as loading control. Representative image from n=2 independent experiments.

Supplementary Figure 4. Relevant to Figure 4.

(**A**) Immunoblot of TrkB in R15 and R24 GSC compared with paired DIFF cells. α-tubulin served as loading control. Representative image from n=2 independent experiments. (**B**) G7 GSC treated with indicated drugs for 24h hours in full stem-cell medium (including EGF and FGF) and analysed for cell viability using an IncuCyte imager and SYTOX Green exclusion. Error bars represent mean +/-SEM from n=3 independent experiments. (ns, p=0.0817) Welch's test. (**C**) G7 DIFF were treated with A-1331852 2μM +/- BDNF (100ng/mL) for 1 hour, harvested and protein expression was analysed by immunoblot (*indicates high

exposure). α-tubulin served as loading control. Representative image from n=3 independent experiments.

Supplementary Figure 5. Relevant to Figure 5.

(**A**) Schematic model of fresh GBM patient tissue collection and processing. (**B**) Quantification of cell reduction in GBM case 1-3 normalised to DMSO-treated control. Error bars represent mean +/-SEM (*p=0.0257) Welch's test. (**C,D**) Representative H&E and Ki67 IHC images of GBM patients case 1 and 2 treated with single inhibitors A-1331852 2μM or S63845 2μM for 72 hours. In both cases H&E control images were used from the same area as shown in Figure 5A,B in different magnification. (**E**) Quantification of SOX2 positive cell reduction in GBM case 1-3 normalised to DMSO-treated control. Error bars represent mean +/-SEM (*p=0.0145) Welch's test. (**F**) Representative images of SOX2 IHC in GBM case 1-3. (**G**) Representative H&E images of GBM case 1-3, arrows indicate intratumoural vessels.

Supplementary Figure 6. Relevant to Figure 6.

(**A**) Immunoblot of E2 and G7 GSC vector^{CRISPR} and BIM^{CRISPR} for BCL-xL, MCL-1 and BIM. Representative images from n=2 independent experiments. α-tubulin served as loading control. (**B**) G7 GSC vector^{CRISPR} and BIM^{CRISPR} treated with DMSO or indicated combination for 24 hours and analysed for cell viability using an IncuCyte imager and SYTOX Green exclusion. Error bars represent mean +/-SD from n=3 independent experiments. (**C**) Representative images of U87MG neurospheres in stem-cell medium under treatment with indicated drugs over a total of 60 hours. Quantification of neurosphere treatment for cell viability using an IncuCyte imager and SYTOX Green exclusion given as mean signal intensity (GCU). One representative of n=3 independent experiments shown. Error bars represent mean +/-SD. (**D**) Clonogenic survival assay of U87MG. Treatment commenced 16 hours after plating 250 cells/well with either DMSO or ABT-263 5μM for 24 hours followed by drug washout and treatment pause for 24 hours and S63845 2μM for 24 hours. Alternating

82 treatment was continued over the experimental period of 14 days. Colonies were counted
83 manually. Quantification of one representative of n=2 independent experiments shown.
84 Representative images of a replicate in one independent repeat scanned on LICOR imager.
85 (**E**) Schematic of treatment schedule for *in vivo* study. (**F**) Percent weight change of mice
86 (vehicle n=6, ABT-236, S63845 n=7) during the drug treatment period of the experiment in
87 Figure 1G,H. (**G**) Representative H&E and Ki67 IHC images of U87MG xenografts treated
88 with vehicle or alternating ABT-263 and S63845 therapy at end point.
89